國立臺灣大學醫學院分子醫學研究所

博士論文

Institute of Molecular Medicine

College of Medicine

National Taiwan University

Doctoral Dissertation

與脂筏交互作用的Galectin8調控初級纖毛生長之研究

Lipid raft interacting galectin 8 regulates primary ciliogenesis

許展彰

Jhan-Jhang Syu

指導教授：周祖述 博士

Advisor: Tuzz-Shuh Jou, Ph.D

中華民國 一一二 年 七 月

July, 2023

doi:10.6342/NTU202302590

國立臺灣大學博士學位論文
口試委員會審定書

與脂筏交互作用的Galectin 8調控初級纖毛生長之研究

Lipid raft interacting galectin 8 regulates primary ciliogenesis

本論文係許展彰君（學號 D04448002）在國立臺灣大學分子醫學研究所完成之博士學位論文，於民國一一二年七月二十一日承下列考試委員審查通過及口試及格，特此證明

口試委員：周祖述（簽名）

（指導教授）

陳佑宗　蔡欣祐

葉秀慧　鄭永銘

系主任、所長　潘俊良（簽名）

中文摘要

在細胞分化後的頂端區域有著一個特殊的胞器稱為初級纖毛。在之前的研究中發現，初級纖毛有別於運動用的纖毛是屬於靜態的、能感知和傳遞環境訊息的胞器，初級纖毛的生成及長度受到各種機制的嚴格調控，例如纖毛的生成及伸長會受到物質在鞭毛內輸送蛋白運輸的頻率或大小來控制，這些輸送蛋白運送材料也包含纖毛生長所必需的微管蛋白和訊息分子等。在本次研究中，我們發現在初級纖毛的細胞膜上被唾液酸聚醣修飾的蛋白質或是脂質與半乳糖凝集素 8 的交互作用會調控初級纖毛的生長。在細胞進行極化的過程中，我們觀察到分泌到細胞頂端區域外部的半乳糖凝集素 8 會隨著時間增加，同時這些細胞外的半乳糖凝集素 8 會結合到初級纖毛及初級纖毛根部的過度區，根據我們的觀察，這樣的結合會使初級纖毛出現快速生長的現象。透過實驗分析，我們發現半乳糖凝集素 8 會和脂筏的組成分子有一定程度的交互關係，如：神經節苷脂和小窩蛋白 1 等，這個結果可以支持我們的假說，即半乳糖凝集素 8 會結合在初級纖毛及初級纖毛根部的過度區。此外我們觀察到半乳糖凝集素 8 結合在初級纖毛後會擾亂初級纖毛過渡區的屏障功能，促使初級纖毛的快速生長。我們的研究還發現，初級纖毛過渡區的屏障功能是否健全取決於初級纖毛過度區中脂筏結構的完整性，在小窩蛋白 1 基因敲除和脂筏的藥理學抑制實驗均表現出類似於頂端添加重組半乳糖凝集素 8 的效果，即初級纖毛快速生長和初級纖毛過度區屏障功能受損，因此我們推論半乳糖凝集素 8 在初級纖毛短期快速生長上扮演一個重要的角色。後續，我們透過轉錄組分析和蛋白質組分析也發現，半乳糖凝集素 8 會和胰島素樣生長因子 1 受體有高度的親和性，同時胰島素樣生長因子 1 受體下游的蛋白激酶 B 被活化、Myc 的訊號路徑活化和 Myc 蛋白質表現量增加，這些都暗示著半乳糖凝集素 8 和初級纖毛的交互作用會誘導細胞重新進入有絲分裂的循環週期。

關鍵詞: 初級纖毛, 初級纖毛過渡區, 脂筏, 神經節苷脂, 半乳糖凝集素 8, 小窩蛋白 1

doi:10.6342/NTU202302590

ABSTRACT

Primary cilium is a specialized sensory organelle that transmits environmental information into cells. Its length is tightly controlled by various mechanisms such as the frequency or the cargo size of the intraflagellar transport trains which deliver the building materials such as tubulin subunits essential for the growing cilia. Here we show the sialoglycan interacting galectin 8 regulates the process of primary ciliogenesis. As the epithelia become polarized, there are more galectin 8 being apically secreted and these extracellular galectin 8 molecules apparently bind to a lipid raft enriched domain at the base of the primary cilia through interacting with lipid raft components ganglioside and caveolin 1. Furthermore, the binding of galectin 8 at this critical region triggers rapid growth of primary cilia by perturbing the barrier function of transition zone. Our study also demonstrates the functionality of this barrier depends on intact organization of lipid rafts at the cilia as genetically knockout of Cav1 and pharmacologically inhibition of lipid raft both phenocopy the effect of apical addition of recombinant galectin 8; i.e., rapid elongation of primary cilia and redistribution of cilial proteins from transition zone to the growing cilial trunk. We also investigated the cellular response after galectin 8 interacted with primary cilia through transcriptome and proteome analysis. The proteomics analysis implied Gal8 might interact with insulin-like growth factor 1 receptor (IGF1R) while the transcriptomic analysis showed Myc signaling pathway was up-regulated. Moreover, the protein kinase B (AKT) which had been reported as a downstream target of IGF1R was activated and the Myc protein level was increased. Our results imply that the interaction of galectin 8 with primary cilia induces cell entry into the cell cycle.

Key words: primary cilia, transition zone, lipid raft, ganglioside, galectin 8, caveolin 1

doi:10.6342/NTU202302590

CONTENT

doi:10.6342/NTU202302590

doi:10.6342/NTU202302590

doi:10.6342/NTU202302590

BBREVIATION

Galectin 8	Gal8
Arl13B	ADP Ribosylation Factor Like GTPase 13B
Ac-tub	Acetylated-alpha-tubulin
γ-tub	Garma-tubulin
His	Histidine
GST	Gutathione S-transferase
AP	Apical domain
BL	Basolateral domain
Flot1	Flotillin 1
Stom	Stomatin
Cav1	Caveolin 1
TZ	Transition zone
TMEM231	Transmembrane protein 231
CTxB	Cholera Toxin B subunit
MBCD	Methyl-beta-cyclodextrin

doi:10.6342/NTU202302590

INTRODUCTION

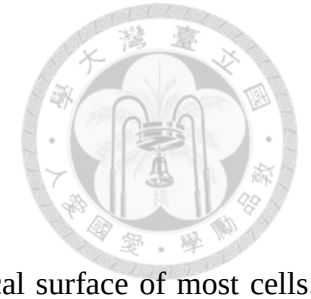

Primary cilia structure and ciliogenesis

Primary cilium is a solitary protruding organelle found at the apical surface of most cells. Ultrastructurally, it can be distinguished as a pole-like structure composed of a so-named 9+0 organized microtubule cylinder axoneme that emanates from a centriole derived structure called the basal body [1] . Primary cilium serves as a specialized sensory hub where intensive signaling can be transduced from outside environmental stimuli to influence various cellular behaviors such as cell cycle progression. Although complex morphology exists in cilia of specific cell types, primary cilia in the majority of cells possess a plain rod-like appearance; therefore, an apparent morphological attribute in most cilia is its length, which is tightly modulated in response to environmental factors such as fluid induced shear force [2].

In many cell types, the first event of primary cilia ciliogenesis is ciliary vesicle docking to mature mother centriole which contains distal and subdistal appendages [3, 4]. The ciliary vesicle binds to distal/subdistal appendages and fuses with secondary vesicles. The transition zone (TZ) begins to emerge and irrupt into the ciliary vesicle simultaneously. This centriole-vesicle complex migrates and fuses with the plasma membrane. During the centriole-vesicle complex migration, intraflagellar transport (IFT) and Bardet–Biedl syndrome (BBS) family proteins, both are specific transporter in primary cilia, would be recruited to ciliary base that make the basal body and TZ maturation [5-7]. At last step, after centriole-vesicle complex fuses to plasma membrane, IFTs transport the cargos into primary cilia and extend the axoneme [8-10].

doi:10.6342/NTU202302590

Cilia formation is governed by a conserved IFT process which is mediated by the balanced interaction between anterograde motor kinesin 2 and retrograde motor dynein with the IFT-B and IFT-A protein complexes [11, 12]. Several models have been proposed for IFT-dependent mechanisms of ciliary length control [13-17] . Most of these models suggest the existence of a molecular gate governing the entry rate of IFT dependent cargo from cytosol into the cilia. Despite the detailed biochemical nature of this hypothetic gate remains elusive, the subcellular location of this gate is believed to be at the TZ region of primary cilia [18, 19].

The function of transition zone on primary cilia

Transition zone (TZ) is defined for the region at the base of the primary cilium where transition fibers/distal appendages anchor the basal body to the ciliary base. The most important function of TZ is regulating the entry and exit of molecules at the primary cilia base [20]. The composition of TZ displays a unique protein and lipid composition contenting ciliary membrane, cilia axoneme, and Y-shaped linkers, which connect microtubules to the plasma membrane [21]. There are several protein families have been reported to be localized at the TZ, including the Meckel syndrome (MKS), Nephronophthisis(NPHP) and Joubert syndrome (JBTS) proteins which are conserved between species and cell-types [22, 23]. Some MKS-related transmembrane proteins (such as TMEM231 and TMEM237) are located on the cilia membrane, and these proteins interact with the Y-shaped linker so that the Y-shaped linker can connect to the microtubule and cilia membrane to stabilize the structure of TZ [20]. A critical defect showing reduced primary ciliogenesis is manifested when the TZ components MKS or JBTS proteins have been inhibited [24]. On the other hand, a previously study demonstrates that inhibiting the KIF13B on TZ does not affect ciliogenesis, but elongates the cilia length [25]. Despite a great number of evidences supporting the role of TZ as a diffusion barrier that can efficiently prevent free mixing of ciliary components with other membranous and soluble molecules from subcellular regions elsewhere of cilia, the biochemical composition of TZ is not well

doi:10.6342/NTU202302590

characterized.

It has been reported that the TZ membrane is the most detergent resistant of all surface membranes in C. reinhardtii [26] suggesting that a high-ordered lipid phase resides at the TZ. This characteristic is reminiscent of the lipid rafts existing at other cellular membranes. Indeed, several studies have shown that the membrane of TZ on primary cilia is a lipid raft reach region[25, 27, 28]. However, whether lipid rafts also play a regulatory role in the TZ region to govern the length of primary cilia remains an interesting issue to be explored.

The galectin 8 and galectin protein families

Galectins are galactose-binding lectins with conserved carbohydrate recognition domains (CRD). Galectins can be categorized into three sub-type relies on the structure and number of CRDs: prototype galectins (Galectin-1, -2, -5, -7, and -10) with one CRD that forms homodimers, chimera type (Galectin-3) with a single CRD and a non-lectin N-terminal domain (NTD) which performs multivalent properties by self-binding; and tandem-repeat type (Galectin-4, -6, -8, -9, and -12) galectins having separate N-terminal and C-terminal CRDs recognizing differential species of galactosides [29].

Galectin 8 has been reported to be more distributed in mammalian tissues than other tandem-repeat type galectins [30]. Galectin 8 also exhibits high transcription levels in MDCK cells [31]. With frontal affinity chromatography analysis [32], Galectin 8 possesses a unique and strong binding affinity to acidic glycolipids, GM3 and GD1a [33]. This feature is attributed to the N-terminal CRD of galectin 8. A recent research has shown that the three amino acids (Arg45, Gln47, and Arg59) on N-terminal CRD of human galectin 8 are important in the interaction of galectin 8 with the sialylated or sulfated oligosaccharides [34]. We have shown that galectin 8 is involved in Gp135/podocalyxin trafficking to the apical domain through interaction with the

doi:10.6342/NTU202302590

extracellular of Gp135 which is an O-glycosylation–rich region [35]. These studies imply that Gal8 prefers to interact with glycosyl groups carrying net negative charges.

Many studies have shown that galectin 8 is involved in several cellular functions and signaling transmission. In Helicobacter pylori-infected human-derived AGS gastric epithelial cells, intracellular galectin 8 aggregates and colocalizes with autophagosomes to enhance the autophagy activity in infected cells [36]. Another study found that extracellular galectin 8 work-together with B lymphocytes to enhance antigen recognition. In this case, the expression of galectin 8 is increased in lymph nodes and facilitates synapse formation under inflammatory conditions. Simultaneously, galectin 8 promotes lysosome recruitment at the B cell-antigen contact site and increases the immobilized antigens extraction [37]. On the other hand, galectin 8 is also involved in several signaling transductions as extracellular unconventional ligands or intracellular regulators. For example, galectin 8 has been found to participate in MAPK signaling and binds to K-Ras4B which regulate cell migration and cell proliferation [38, 39]. However, the function of galectin 8 on primary cilia remains to be clarified. Thence, we set up to decipher the role of galectin 8 in primary cilia.

The cell signaling on primary cilia

On primary cilia, the ciliary membrane is enclosed which included unique lipid and receptor composition. There are several signaling has been repot that regulated cellular physiology, such as Hedgehog signaling, Wnt/β-catenin signaling and AKT signaling [40].

The primary cilia are the major platforms of Hedgehog signaling transduction in vertebrates. Without stimulation, Ptc1, a transmembrane receptor of sonic hedgehog (Shh), localizes on the cilia membrane that restricts and excludes Smoothened (Smo) translocate into the cilium axoneme to interact with Suppressor of Fused (SuFu), a suppressor of transcription factors Gli.

doi:10.6342/NTU202302590

With Shh stimulation, Ptc1 binds to Shh and leaves the cilium ensuring Smo enters into the cilium to repress SuFu and release Gli. Then released Gli is post-translationally modified to GliA and transported to nucleus to activate the downstream genes [41, 42].

Wnt/β-catenin signaling is a pivotal signaling pathway in embryonic development and adult tissue homeostasis. Without Wnt stimulation (inactivation), β-catenin is arrested and degraded by glycogen synthase kinase-3β, Axin, and Adenomatous polyposis coli protein complex. When Wnt ligands bind to transmembrane receptor Frizzled, the lipoprotein receptor-related protein recruits Axin to the plasma membrane and releases β-catenin. The free β-catenin is translocated into nuclease with the assistance of Ahi and binds to TCF/LEF transcription factors that promote downstream gene expression. The role of primary cilia in Wnt signaling is thought to be an inhibitor that represses the Dvl to prevent Axin recruited to the plasma membrane and arrests Ahi in cilia axoneme to reduce β-catenin entry into the nucleus [43, 44].

The previously study about stem cell reported that primary cilia elongation should recruit IGF1Rβ to the cilia membrane during adipogenic differentiation in human mesenchymal stem cells [45]. In 3T3-L1 adipocyte differentiation model, similar result is found the that the primary cilia formation is critical in adipocyte differentiation. During primary cilia formation, insulin receptor substrate 1, a downstream molecular of IGF1R, is recruited to primary cilia basal body and actives AKT1 [46]. Both of these two studies imply that primary cilia formation and elongation is associated with IGF1R-AKT signaling. Several evidences suggest that complicated signaling components within the cilium are dynamic to reflect the environment and the differentiation of the cells [47]. However, the implication of primary cilia elongation in cell signaling is still unclear. Thus, we want to investigate the relationship of the primary cilia length and the cellular response during cilia elongation.

doi:10.6342/NTU202302590

In current study, we provided reinforcing evidences that lipid rafts like domain exists at the base of primary cilium and plays a regulatory role in controlling the length of primary cilia. Furthermore, galectin 8 (Gal8), a ganglioside specific beta-galactoside binding lectin type protein, can be secreted from polarizing epithelia and promote ciliogenesis, through its interaction with caveolin 1 and ganglioside, two of the instrumental components of lipid rafts.

doi:10.6342/NTU202302590

METHODS AND MATERIALS

Cell Culture

Madin-Darby canine kidney (MDCK) type II cells were cultured in DMEM supplemented with 10% fetal bovine serum and penicillin/streptomycin/ampicillin at 37°C in a humidified incubator containing 5% CO2. To generate Gal8 knocked down MDCK clones, cells were transfected with the siRNA-expressing vector using Lipofectamine 2000 (#11668019, Invitrogen, Thermo Fisher Scientific, Waltham, Massachusetts, U.S.) according to the manufacturer's instructions before selection at 0.25 mg/ml hygromycin B (#400052, Calbiochem, Merck, Darmstadt, Germany). For the ciliogenesis-related assay, MDCK cells were plated as an instant monolayer and allowed to be polarized in 12 mm Transwell (#3401, Corning, New York, U.S.) for 7 days or for the indicated period specified in the relevant figure legends.

Antibodies and chemicals

The following antibodies were used in this study: rabbit anti-galectin 8 (ab69631, Abcam, Cambridge, UK), rabbit anti-caveolin 1 (#3267, Cell Signaling Technology, Massachusetts, U.S.), rabbit anti-caveolin 1 (1644-1-AP, Proteintech, Chicago, U.S.), rabbit anti-acetylated alpha-tubulin (#5335, Cell Signaling Technology), rabbit anti-GST (#2625, Cell Signaling Technology), mouse anti-flotillin 1 (#610821, BD Transduction Laboratories, Franklin Lakes, New Jersey, U.S.), rabbit anti-TMEM231 (HPA042081, Sigma-Aldrich, Merck, Darmstadt, Germany), rabbit anti-INPP5E (AP58228, abcepta, California, U.S.), rabbit anti-AKT (#9272, Cell Signaling Technology), rabbit anti-phosphorylated AKT (S473) (#9271, Cell Signaling Technology), rabbit anti-GSK3β (S9) (#9336, Cell Signaling Technology), mouse anti-ganglioside GD3 (MAB2053, Merck), mouse anti-ganglioside GD1a, GD1b-1, GM1-2b, GT1b-2a (Developmental Studies Hybridoma Bank), mouse anti-stomatin (sc-376920; Santa

doi:10.6342/NTU202302590

Cruz Biotechnology, Texas, USA), mouse anti-caveolin 1 (66067-1-Ig, Proteintech), mouse ant-myc (5E9G2) (TA507203, Origene), mouse anti-acetylated alpha-tubulin (T6793; Sigma-Aldrich), mouse anti-His (27E8) (#2366, Cell Signaling Technology). The following chemicals were used in this study: calcium chloride ($CaCl_2$) (C4901, Sigma-Aldrich), magnesium chloride hexahydrate ($MgCl_2 \cdot 6H_2O$) (#31413, Sigma-Aldrich), lovastatin (#438185, Sigma-Aldrich), methyl-β-cyclodextrin (MBCD) (C4555, Sigma-Aldrich).

Plasmids construction and recombinant protein purification

The wild type Gal8 cDNA were amplified from the reverse transcribed products of MDCK cells with PCR using the followed specific primers: forward: 5'-GCGGATCCATGTTGTCCTTAAA AAACCTGCAG-3', reverse: 5'-GCGGATCCCAGCTCCTTACTTCCAGT-3', containing a BamHI restriction site respectively. The purified PCR product was cleaved using endonucleases BamHI (New England Biolab, Massachusetts,, U.S.) and was ligated into the pET15b or pGEX6 vector respectively to construct the plasmid expressing histidine (His)-tagged or Glutathione-S-transferase (GST)-tagged recombinant Gal8 protein. To generate alanine scanning mutants, the plasmid harboring wild type Gal8 cDNA was used as a template to go for 3 sequential rounds of site-directed mutagenesis in order to generate a $Arg^{44}Ala/Gln^{46}Ala/Arg^{58}Ala$ recombinant constructed in the pGEX6 vector (GST-Gal8-AAA mutant) using 3 pairs of primers with the following base sequences: Gln^{46} to Ala^{46} forward: 5'-CTTGTGATTCAGACAGGTTCGCGGTGGACCTGCA-3', reverse: 5'-TGCAGGTCCACC GCGAACCTGTCTGAATCACAAG-3', Arg^{58} to Ala^{58} forward: 5'-GCGTGAAGCCAGCCGC CGACGTGGC-3', reverse: 5'-GCCACGTCGGCGGCTGGCTTCACGC-3', Arg^{44}/Ala^{46} to Ala^{44}/Ala^{46} forward: 5'-CTTGTGATTCAGACGCCTTCGCGGTGGACC-3', reverse: 5'-GGTC CACCGCGAAGGCGTCTGAATCACAAG-3'. All the above constructs were sequence verified. The expression and purification of His-Gal8 was performed as previously reported for His-tagged proteins [48]. The plasmids were transformed into Escherichia coli BL21 strain

doi:10.6342/NTU202302590

which was then incubated in LB broth (#12780-052, Invitrogen) supplemented by 100 μg/ml carbenicillin (C1389, Sigma-Aldrich) at 37°C overnight. The overnight culture was diluted in next morning with fresh LB broth (v/v = 1:10) and incubated further until the OD_{600} reached 0.8. Isopropyl β-D-1-thiogalactopyranoside (IPTG, #15529019, Thermo Fisher Scientific) of 0.5 mM was added to the bacterial culture which was incubated at 37°C for another 2 h. Bacteria were harvested by centrifugation (3,000×*g*, 10 min, 4°C) and re-suspended in cold lysis buffer (50 mM Tris, pH 7.5, 1% Triton X-100, 150 mM NaCl, 5 mM $MgCl_2$) with proteinase inhibitor. Re-suspended bacteria were frozen and thawed three times and were then sonicated (22 amplitude microns for three times, 10 sec each pulse with 1 min pause between sonication) on ice. Bacterial lysate (supernatant) was harvested by centrifugation (16,000×*g*, 30 min, 4°C). Prepared appropriate volume (v/v = 1:9) glutathione sepharose beads 4B (GE17-0756-01, GE Healthcare, Chicago, U.S.) wash with lysis buffer 3 times and removed excess buffer. Bacteria lysate mixed with prepared sepharose beads 4B rotated at 4°C overnight. GST recombinant proteins were eluted by 0.2 μM L-Glutathione reduced (G4251, Sigma-Aldrich) and concentrated/desalted with Amicon Ultra-4 (UFC801096, Merck) according to the manufacturer's instructions.

Generation of a MDCK clone stably expressing Arl13B-mCherry

The plasmid (gift of Dr. Yu-Chun Lin) expressing mouse Arl13B C-terminally tagged with mCherry was transfected into MDCK cells using Lipofectamine 2000 (#11668019, Invitrogen) according to the manufacturer's instructions. The transfected cells were selected with 0.8 mg/ml G418 for two weeks before the surviving candidates were pooled and subjected for two rounds of fluorescence-activated cell sorting by the FACSAria™ III (BD Biosciences) to enriched the mCherry-positive cells to more than 95% in the cell population.

doi:10.6342/NTU202302590

GST fused Gal8 pull-down assay and Western blot

The GST-fused full-length Gal8 were produced in Escherichia coli BL21 strain and conventionally purified on glutathione-Sepharose 4B beads (GE17-0756-01, GE Healthcare). MDCK cells were lysed in CSK buffer (50 mM NaCl, 300 mM sucrose, 10 mM PIPES (pH 6.8), 3 mM $MgCl_2$, and 0.5% (v/v) Triton X-100) and incubated overnight at 4°C with GST fused Gal8 captured on Sepharose 4B beads. The beads were then washed with CSK buffer 3 times with intermittent sedimentation by centrifugation. Pulled-down proteins were collected by boiling in SDS sample buffer. Then, the samples were resolved by SDS-PAGE and analyzed by Western blotting. For Western blotting, proteins were blotted onto nitrocellulose membranes (NBA085C001EA, PerkinElmer, Massachusetts, U.S.) which were blocked in 5% milk/PBS containing 0.05% (v/v) Tween-20 (PBST). The membranes were incubated with primary antibody overnight at 4°C followed by 3 washes with PBST and vigorous shaking. The membranes were incubated with horseradish peroxidase-conjugated secondary antibodies (NA931V or NA934V, GE Healthcare) at room temperature for 1 h, and visualization was performed using enhanced chemiluminescence reagents (PK-NEL122, PerkinElmer) and exposure to X-ray film (GE28-9068-39, GE Healthcare).

Immunoprecipitation of Gal8 secreted in the culture medium

The FLAG-Gal8 stably expressing MDCK cells were cultured on 24 mm Transwell (#3412, Corning), and then apical and basolateral culture medium was collected on the predetermined dates (2, 6, 8, and 10 days). Collected cultured media were incubated with mouse anti-FLAG antibody conjugated agarose beads (A2220, Sigma-Aldrich) and rotated at 4°C overnight. The immunoprecipitated materials were separated by SDS-PAGE followed by Western blotting analysis using appropriate antibodies.

doi:10.6342/NTU202302590

Lipid-binding assay

Sphingo strips (S-6000, Echelon Biosciences) were incubated with His- or GST-Gal8 for 1 h at room temperature. The membranes were blocked in 5% milk/PBS containing 0.05% (v/v) Tween-20 (PBST). The membranes were incubated with primary antibody overnight at 4°C followed by 3 washes with PBST and vigorous shaking. The membranes were incubated with horseradish peroxidase-conjugated secondary antibodies (NA931V or NA934V, GE Healthcare) at room temperature for 1 h, and visualization was performed using enhanced chemiluminescence reagents (PK-NEL122, PerkinElmer) and exposure to X-ray film (GE28-9068-39, GE Healthcare).

Lipid floatation assay

Confluent MDCK cells grown on 75 mm Transwell (#7910, Corning) were lysed for 20 min on ice in 2 ml of TNE buffer (20 mM Tris-HCl, pH 7.5, 150 mM NaCl, 5 mM EDTA) containing 1% Triton X-100 and passed five times through a 26-gauge needle. The 2 ml lysate was mixed with 2 ml 80% sucrose in TNE and placed at the bottom of a centrifuge tube (331372, 14 X 89 mm, Beckman Coulter). A discontinuous sucrose gradient (5–30% in TNE) was layered on top of the lysates, and the samples were centrifuged at 39,000 rpm for 18 h in an ultracentrifuge (SW41; Beckman Coulter, Brea, California, U.S.). The fractions were separated by SDS-PAGE followed by Western blotting analysis using appropriate antibodies.

Immunofluorescence staining and microscopy

MDCK cells cultured on 12 mm Transwell (#3401, Corning) were washed twice with PBS containing Ca^{2+} and Mg^{2+} (phosphate-buffered saline containing 1 mM $CaCl_2$ and 0.5 mM $MgCl_2$) and fixed with 3.7% (w/v) paraformaldehyde. Permeabilization was carried out by incubation with CSK buffer at room temperature for 15 min. Cells were then washed twice with PBS and blocked with PBS containing 1% (w/v) bovine serum albumin (BSA), 10% (v/v) goat

doi:10.6342/NTU202302590

serum, and 50 mM NH_4Cl at room temperature for 1 h. After washing briefly with PBS containing 0.2% (w/v) BSA, the cells were incubated with primary antibody overnight at 4°C. Cells were then washed thrice with PBS containing 0.2% (w/v) BSA and incubated with secondary antibody at room temperature for 2–4 h. After washing thrice with PBS containing 0.2% (w/v) BSA, cells were mounted with ProLong™ Diamond Antifade Mountant (P36961, Thermo Fisher Scientific). Images were acquired with a Zeiss LSM880 confocal microscope (Carl Zeiss, Jena, Germany).

The mouse tissue section staining was followed: paraffin sections of mouse kidney tissue were deparaffinized, rehydrated, and autoclaved in Trilogy™ (920P-06, Cell Marque, Rocklin California, U.S.) for antigen retrieval before being permeabilized with CSK buffer for 15 min. Then, the sections were washed twice with PBS, 5 min each, and blocked in blocking solution (PBS containing 1% BSA, 10% goat serum, and 50 mM NH_4Cl) for 1 h followed by washing twice with PBS containing 0.2% BSA. Sections of the kidneys were incubated with primary antibody at 4°C overnight, were washed three times, each for 5 min, in PBS containing 0.2% BSA, and were incubated with a secondary antibody which is goat anti-mouse or rabbit with fluorescein-conjugated for 90 min at room temperature in the dark. Sections of kidney were washed three times, each for 5 min, in PBS containing 0.2% BSA, and mounted with ProLong™ Diamond Antifade Mountant (P36961, Thermo Fisher Scientific).

Surface biotinylation and mass spectrometry

MDCK cells were cultured on 75 mm Transwell (#7910, Corning) for 7 d for polarization. Transepithelial electric resistance was measured each time before performing the experiments to confirm the tightness of the monolayer. Filters were washed three times with cold PBS containing Ca^{2+} and Mg^{2+}. Sulfo-NHS-biotin (#21217, Thermo Fisher Scientific) in PBS containing Ca^{2+} and Mg^{2+} was applied to apical (4 ml) chambers. Filters were incubated on ice for 30 min on a rocker platform. Unreacted biotin was quenched by washing cells in five changes

doi:10.6342/NTU202302590

of Tris-saline (10 mM Tris-HCl, pH 7.4, 120 mM NaCl). Then each filter was incubated with 4 ml of GST-Gal8 (0.1 μg/μl) on ice for 30 min on a rocker platform. After washing by three changes of cold PBS, the cells were then extracted in CSK buffer for 15 min at 4°C. Cell lysates were centrifuged (12,000×*g*, 10 min) and the collected supernatant was then incubated with glutathione sepharose beads (GE17-0756-01, GE Healthcare) at room temperature for 3 h. Beads would be washed three times with PBS and eluted twice with elution buffer (50 mM Tris-HCl, 10 mM reduced glutathione, pH 8.0). The eluted lysates were incubated with immobilized avidin (＃20219, Pierce, Thermo Fisher Scientific) overnight at 4°C. The collected beads were washed with PBS 3 times before adding with 2x SDS sample buffer (v/v) and resolved by SDS-PAGE. The gel was then silver stained, followed by in-gel tryptic digestion and liquid chromatography-tandem mass spectrometry as described previously [49, 50]. To identify the protein, the raw spectrometry data were analyzed using Proteome Discoverer software (version 1.4, Thermo Fisher Scientific). The resulting mass spectra were searched against Swiss-Prot Canis sequence database using the Mascot search engine (Matrix Science, version 2.2.04). The annotated subcellular localization of our identified proteins was according to the Ingenuity Pathway Analysis (IPA, Qiagen) software. Proteomic data for the Gal8 interactome have been deposited in the ProteomeXchange Consortium (http://proteomecentral.proteomexchange.org) through the PRIDE partner repository (https://www.ebi.ac.uk/pride/) [51]. The dataset identifier is PXD038021.

Lipid raft labeling with Cholera toxin subunit B

MDCK cells cultured on 12 mm Transwell (#3401, Corning) were washed twice with PBS containing Ca^{2+} and Mg^{2+} and incubated with Cholera toxin subunit B (C22843, Invitrogen) on apical space for 30 min on ice. After then, cells were fixed with 3.7% (w/v) paraformaldehyde for 15 min kept on ice, and permeabilized with CSK buffer for 15 min at room temperature. Cells were then washed twice with PBS and blocked with PBS containing 1% (w/v) bovine

doi:10.6342/NTU202302590

serum albumin (BSA), 10% (v/v) goat serum, and 50 mM NH4Cl at room temperature for 1 h. After washing briefly with PBS containing 0.2% (w/v) BSA, the cells were incubated with primary antibody overnight at 4°C. Cells were then washed thrice with PBS containing 0.2% (w/v) BSA and incubated with secondary antibody at room temperature for 2–4 h. After washing thrice with PBS containing 0.2% (w/v) BSA, cells were mounted in ProLong™ Diamond Antifade Mountant (P36961, Thermo Fisher Scientific). Images were acquired with Zeiss LSM880 confocal microscope (Carl Zeiss).

The lipid raft perturbation treatment

MDCK cells were cultured on 12 mm Transwell (#3401, Corning) co-treated with 5 mM lovastatin (#438185, Sigma-Aldrich) and 2.5 mM MBCD (C4555, Sigma-Aldrich) at 37°C for 1 h. The cells were washed twice with PBS and preceded as described above for immunofluorescence staining. The images were acquired with Zeiss LSM880 confocal microscope (Carl Zeiss).

CRISPR/Cas9 knockout Cav1

The targeting sequences of gRNA for Cas9 were the following: Cav1 5'-GGTGTACGACGCGC ACACCA-3'; 5'-CAAGCATCTCAACGACGACG-3'. The gRNAs which were generated by inserting annealed primers were inserted into the gRNA/Cas9/GFP cloning vector (plasmid #PX458, Addgene). The plasmids were transfected to MDCK cells and generated the stably knockout single clone. The single colonies of MDCK cells were screened and collected by flow cytometer (Fluorescence-activated cell sorting). The knock-out cell lines were analyzed by western blotting, confocal immunofluorescence microscopy, and DNA sequencing.

Transcriptomic analysis and next-generation sequencing (NGS)

MDCK G cell were cultured on 12 mm Trnaswell (#3401, Corning) and pre-treat with GST only or GST-Gal8 on ice for 30 min. After removed GST or Gal8, cells were washed and recovery

doi:10.6342/NTU202302590

with fresh completed medium in 37°C for 5 h. Cells were lysed with TRIzol (#15596026, Thermo Fisher Scientific) and isolated total RNA according to the user guide of TRIzol. The RNA samples were commissioned the sequencing core laboratory of the second core laboratory of National Taiwan University Hospital for next-generation sequencing and analysis.

EdU staining and cell proliferation rate assay

MDCK cells were cultured on 12 mm Transwell (#3401, Corning) and pre-treat with GST only or GST-Gal8. Cells were washed twice with PBS containing Ca^{2+} and Mg^{2+} and used Click-iT™ EdU Cell Proliferation Kit (C10339, Thermo Fisher Scientific) to label the proliferated cell. The steps of EdU staining were according to the user guide manuals. Cells were mounted with ProLong™ Diamond Antifade Mountant (P36961, Thermo Fisher Scientific). Images were acquired with a Zeiss LSM880 confocal microscope (Carl Zeiss).

Quantification of primary cilia length and statistical analyses

The 3D reconstructions of images were generated using microscope software Zen 2011 (Carl Zeiss) and quantification of cilia length in the 3D was made with Fiji as an image processing package (National Institutes of Health, Bethesda, MD, USA). The data of primary cilia length are quantified with nonparametric test with GraphPad Prism 7. Continuous data are presented as median with interquartile range deviations. Differences in the values between two groups were determined by Student's t-test or Mann–Whitney U test. When more than two groups were compared, one-way ANOVA or Kruskal-Wallis test was performed, and a value of $P < 0.05$ was considered statistically significant. Densitometry analysis was carried out using ImageJ.

doi:10.6342/NTU202302590

RESULTS

PART I. Galectin 8 promoted primary cilia elongation

In a previous study, we found that knock down Gal8 decreases primary cilia number on the cell apical domain. In part I, we wanted to investigate how Gal8 interacted with primary cilia and affected primary ciliogenesis.

Extracellular galectin 8 interacted with primary cilia membrane and promoted cilia elongation in polarized MDCK monolayer.

While we reported the effect of Gal8 knockdown on the apical-basal polarity of MDCK cells via apical targeting of Gp135/podocalyxin [35], we also noticed that there was an accompanying decrease of ciliated cells in the MDCK clones stably knocked down of Gal8 (Fig. 1 A-C). Furthermore, endogenous Gal8 was demonstrated to be distributed in a punctate pattern along the primary cilia (Fig. 2). Based on these results and galectin family proteins are released from cells via a non-canonical secretory pathway [52], we hypothesized that Gal8 interacted with primary cilia as an autocrine/paracrine factor and contributed to the ciliogenesis process during epithelial morphogenesis. To verify this hypothesis, we first examined the exact location of endogenous Gal8 at primary cilia in a MDCK clone stably expressing mouse Arl13B, which is a primary cilia marker, with C-terminally tagged mCherry. The cells were processed for immunostaining using two different experimental protocols: one group of cells were fixed and permeabilized, while the other group of cells would be fixed without permeabilization. As noted earlier, the endogenous Gal8 was colocalized with primary cilia marker acetylated tubulin in permeabilized Arl13B-mcherry MDCK cells (Fig. 3 upper). However, only the Gal8, but not the acetylated tubulin signal could be detected at primary cilia in non-permeabilized Arl13B-mcherry MDCK cells (Fig. 3 lower). The above result demonstrated the non-permeabilization protocol successfully prevented the access of the staining antibodies to intracellular targets such as acetylated tubulin, and further indicated that there was a significant

doi:10.6342/NTU202302590

pool of endogenous Gal8 interacted with primary cilia from extracellular space. Next, we added sub-micromolar recombinant His-tagged Gal8 on the apical domain of polarized MDCK monolayer with the initial goal to see the retention of the exogenous Gal8 at primary cilia. Very surprisingly, we not only observed the signal of recombinant Gal8 retained at primary cilia, but also witnessed the length of primary cilia increased dramatically within several minutes after Gal8 treatment (Fig. 4). We then applied another recombinant protein GST-tagged Gal8 to either the apical or basolateral compartment of polarized MDCK cells, and the length of primary cilia increased only when exogenous GST-Gal8 was presented to the apical domain (Fig. 5A and 5B). Taken together, these results implied that endogenous Gal8 could be secreted to the apical domain and promoted primary cilia elongation in polarized epithelial cells.

This cilia-lengthening effect can be discernable when as low as 5 ng/μl (equal to 0.135 μM) of the recombinant His-Gal8 protein was added to polarized MDCK cells (Fig. 6A and 6B). When we examined the exogenous Gal8 treated cells at earlier time points, there were several unique structures which could be distinguished by acetylated tubulin staining (Fig. 7A-7D). At first, the basal body region ballooned which looked like an “onion”. Then, while these onion-like structures were decreasing their own sizes, there were beads like structures appearing on the elongating primary cilia. Finally, those onion and rosary structures were transforming to those lengthy primary cilia we reproducibly observed 30 min after recombinant Gal8 protein treatment (Fig. 4 and 5A). Besides MDCK cells, the recombinant Gal8 protein also displayed cilia lengthening effect on mouse IMCD3 or NIH3T3 fibroblasts (Fig. 8A and 8B). To further investigate the effect of Gal8, the recombinant Gal8 protein was washed off the apical chamber of the Transwell after incubation for 30 min. Then, the apical chamber was replete with fresh completed medium. We observed that the Gal8-induced lengthening effect on primary cilia would be quite lasting as primary cilia were still longer than the untreated control at 4 hours after recovery (Fig. 9).

doi:10.6342/NTU202302590

Apical domain Gal8 increased in vitro MDCK cell culture and in vivo murine developing renal tubules during the course of cilia lengthening.

It has been reported the primary cilia of MDCK cells elongated over the time course of culturing [53]. As we demonstrated earlier that extracellular Gal8 might play an instrumental role in ciliogenesis, we set to examine whether apically secreted Gal8 would increase during cell culture. To this end, we collected the culture media from the apical and basolateral compartments of a polarized MDCK cell line that stably expressed FLAG-Gal8 [54] and quantified the content of extracellular FLAG-Gal8 after immunoprecipitation of the culture media with mouse anti-FLAG antibodies. We found that increasing Gal8 was transported to the apical pole over cultivation time (Fig. 10A and 10B). The length of primary cilia also elongated during this observation period (Fig. 11A-11C). To address whether the above findings from the in vitro MDCK cell model reflected the scenario in animal tissues, we next studied the developing kidneys. Indeed, endogenous Gal8 exhibited a time dependent accumulation in the renal tubular lumen of developing murine kidneys (Fig. 12A). Furthermore, the ciliated cells (Fig. 12B), length of primary cilia (Fig. 12C) and the endogenous Gal8 puncta (Fig. 12D) all increased over the developmental course in differentiating renal tubular cells. These results indicated that Gal8 was secreted to apical domain in polarizing renal epithelia over a developmental course when primary cilia drastically increased their numbers and lengths.

Gal8 interacted with membranous ganglioside to promote primary cilia elongation.

Previous research demonstrates that Gal8 is distinguished from other galectin family proteins by possessing a preferential affinity for negative-charged oligosaccharides, the sulfated and sialylated glycoconjugates [34]. To explore whether this characteristic is responsible for the interaction between the extracellular Gal8 and its receptive partners over the surface of primary cilia, we applied the recombinant Gal8 proteins to polarized MDCK monolayer grown on

doi:10.6342/NTU202302590

Transwell at 4°C so that the retention signal after washing off the labeling solution might only reflect the surface pool of extracellular Gal8 but not the endocytosed pool. Compatible with our previous results (Fig. 2), there were clear signals of the recombinant proteins at the primary cilia. While addition of GST-Gal8 recombinant protein onto the apical domain of polarized MDCK monolayer resulted in significant anti-GST antibody labeling to the primary cilia, a triple alanine mutant (R44A/Q46A/R58A) of the recombinant Gal8, which was reported to diminish the affinity of Gal8 towards sialic acid containing glycan [34], showed much diminished signals retained at primary cilia(Fig. 13A-13C). To delineate how Gal8 interacted with the primary cilia membrane, we used dot blot assay to identify which lipid species had a relatively strong binding affinity with Gal8. As noted, recombinant GST-Gal8 and His-Gal8 both displayed a specific affinity to negatively charged lipids, especially the disiaganglioside GD3 (Fig. 14). Gangliosides are glycosphingolipid with several sialic acids linked on the β-D-galactose or N-Acetyl-β-D-galactosamine (GalNAc) of glycan chain which are enriched on neurons [55, 56] and are a component of lipid raft [57]. This result showed that Gal8 interacted with ganglioside GD3 in vitro. Moreover, we also observed GD3 was mostly located at the base of primary cilia in polarized MDCK cells, and the endogenous GD3 was redistributed into the shaft of the elongated cilia after addition of recombinant Gal8 in a chaotic pattern (Fig. 15). In fact, all the gangliosides we examined, except GD2, were noted at primary cilia as revealed by their high degree of co-localization with the ciliary marker acetylated tubulin (Fig. 16). We therefore suspect that the gangliosides on primary cilia serve as the docking molecules for the extracellular Gal8 and this interaction is essential for the Gal8 dependent primary cilia elongation. To verify this hypothesis, we saturated first on the cell apical domain of polarized MDCK cells with various ganglioside antibodies at 4°C before application of recombinant Gal8 protein. After GD1a, GD1b, or GT1b antibody pre-treatment, the Gal8 induced primary cilia elongation was significantly deterred; however, the Gal8 elicited ciliary lengthening was not affected by GM1 antibody blocking (Fig. 17A and 17B). Our results indicated that apical Gal8 interacted with

doi:10.6342/NTU202302590

gangliosides on the primary cilia membrane to induce cilia elongation.

Gal8 perturbed a lipid raft based barrier to promote primary cilia elongation.

In addition to membranous gangliosides as the potential candidate for binding apical Gal8, we searched for the protein substrates which Gal8 interacted with on the primary cilia. As the cilia occupy only 0.3% volume of the cell body, traditional biochemical purification scheme, such as pulled down analysis using whole cell lysate would be unsatisfactory to reveal the specific binding partner at the cilia for Gal8, which is known to be localized mainly in the cytosol and likely interacts with many potential interacting partners located at other subcellular compartments outside of primary cilia. To identify the ciliary molecule which mediates the cilia-lengthening effect of Gal8, we approached by adopting sequential apical domain selective biotinylation, surface GST-Gal8 fusion protein incubation, followed by two-step affinity purification scheme (Fig. 18). We then processed these apical surface Gal8-interacting candidates by mass spectrometry. We totally identified 254 reproducible candidates in two independent experiments. There were 96 and 117 plasma membrane candidates noted from the first and second experiments respectively. We focused on 66 candidates categorized as plasma membrane proteins (~25% of total candidates) (Table 1) which were repetitively identified in two separate experiments (Fig. 19). Because we previously established that Gal8 interacted with gangliosides which were components of the lipid raft, candidates of lipid raft scaffold proteins, such as flotillin 1 (Flot1), stomatin (Stom), and caveolin 1 (Cav1), especially drew our attention. To examine whether Gal8 interacted with lipid raft scaffold proteins, Flot1, Stom and Cav1 were over-expressed in HEK293T cells, respectively and mixed with GST or GST-Gal8 beads for pull down assay. Since the result demonstrated that the purified GST-Gal8 recombinant protein can interact with the exogenously expressed HA-Flot1, Stom-FLAG, or Cav1-V5 (Fig. 20A), we sought for further biochemical evidence of Gal8 interacting with lipid raft using flotation assay which revealed that Gal8 co-migrated with endogenous Flot1 and Cav1 lipid raft scaffold proteins (Fig. 20B). Lipid rafts are enriched in TZ region of primary cilia [58]. To demonstrate

doi:10.6342/NTU202302590

the potential interaction between endogenous Gal8 and the lipid rafts at primary cilia in vivo, we labeled live MDCK cells with cholera toxin B subunit (CTxB), a lipid raft marker, before fixating the cells and processing for double immunofluorescence study using mouse anti-acetylated tubulin and rabbit anti-Gal8 antibodies. Interestingly, the CTxB staining was noted at the base of stubby primary cilia with minimal Gal8 nearby (Fig. 21, upper row); however, pronounced Gal8 staining was co-localized with the CTxB signal that was distributed at the bases of other longer primary cilia (Fig. 21A and 21B). Furthermore, there was a close correlation between the staining intensity of endogenous Gal8 that was colocalized with CTxB signal and the length of the respective cilium which was rooted at the same region (Fig. 21C). TMEM231 is a TZ component which has been demonstrated to contribute an essential role for maintaining the TZ ultrastructure and the gatekeeper to regulate cilia transportation [59]. The subcellular localization of TMEM231 was noted to be re-distributed into the elongated cilia upon apical addition of recombinant GST-Gal8 as compared to be located at the cilia base of control cells (Fig. 22). These results implied that the base of the primary cilia (presumably at the transition zone, TZ) could be a lipid raft-enriched region and binding of the apically secreted Gal8 might elicit relocation of TZ component proteins such as TMEM231 and thereby perturb the function of TZ as a cilia transportation barrier to facilitate primary cilia elongation.

Cav1 organized a lipid raft barrier on transition zone to restrict primary cilia growth

The TZ membrane at the base of cilia is the most detergent resistant of all surface membranes in C. reinhardtii [26], and high-ordered lipid phase exists at the transition zone to limit free lateral diffusion of membrane proteins and lipids between ciliary and plasma membranes. It has been shown that knockout of KIF13B, a key regulator of ciliary TZ configuration and membrane composition, led to lipid raft scaffold protein Cav1 translocated from TZ to primary cilia axoneme [25]. Since we demonstrated that the interaction with lipid raft component ganglioside was critical to the cilia-lengthening effect of Gal8 and lipid raft marker

doi:10.6342/NTU202302590

CTxB was located at the bases of primary cilia, we set up to examine the effect of acutely inhibiting lipid raft on cilia length as well as the location of lipid raft scaffold proteins. When MDCK cells were treated with lovastatin and methyl-b-cyclodextrin (MBCD) to inhibit cholesterol biochemical synthesis and deplete cholesterol on lipid raft, primary cilia increased their lengths and Cav1 was re-distributed into the shaft of these elongated cilia (Fig. 23, MBCD). Since we had demonstrated the membrane at the bases of primary cilia, presumably the TZ region, were enriched with lipid rafts and we also identified lipid raft organizing proteins as the apical Gal8 interacting partners, we hypothesize that primary cilia TZ is a lipid raft rich region and extracellular Gal8 binding to TZ would perturb the molecular organization and function there to allow fast elongation of primary cilia. Compatible with this hypothesis, apical application of either the purified recombinant His-Gal8 (Fig. 24A) or GST-Gal8 (Fig. 24B) would induce Cav1 relocation into axoneme of the elongated primary cilia, which phenocopied the pattern observed in cells being depleted of lipid rafts. To further confirm the role of Cav1 in the effect of Gal8 on facilitating cilia growth, we generated Cav1 knock-out MDCK cell lines using CRISPR-Cas9 technology. After DNA sequencing analysis, we identified several candidates and one clone which preserved the wild type genomic sequence. Subsequent Western blotting analysis showed intact Cav1 expression in the clone which apparently preserved the Cav1 genomic sequence (Fig. 25, clone #26); therefore, this clone was used for later study as a mock control. All the other candidates showed much reduction in Cav1 expression with two clones (Fig.25, clones #21 and #41) showed a faint signal at the region of where the endogenous Cav1 was supposed to be on the Western blot. To avoid ambiguity, we selected the two clones (Fig. 25, clones #17 and #31) which displayed a complete absence of Cav1 expression for further assays. Immunofluorescence analysis demonstrated Cav1 expression was located at the base of primary cilia in the mock while there was a complete loss of staining signal in the Cav1 knockout clones (Fig. 25C). Quantitation further confirmed the primary cilia length increased in the Cav1 depleted MDCK cell lines (Fig. 25D). All together, these results revealed that the TZ of

doi:10.6342/NTU202302590

primary cilia was a lipid raft rich region which was organized by Cav1 and Gal8 binding to TZ affected lipid raft structure to facilitate cilia growth.

PART II. Extracellular galectin 8 promoted cell proliferation

In the Part I research, we found a fast morphological change that Gal8, which interacted with the lipid raft on the ciliary membrane, induced primary cilia elongation. It is an interesting issue of how primary cilia elongation affects the physiological mechanisms in MDCK cells. Thus, MDCK cells were treated with Gal8 on the apical domain, and then the non-specifically bound Gal8 was washed away. After that, Cells were recovered at 37°C with complete medium for 5 hour. The mRNAs that were extracted from recovered MDCK cells were analyzed by Next Generation Sequencing (NGS) to investigate what primary cilia-interacted Gal8 regulated signaling mechanisms in MDCK cells.

Apical Gal8 interacted with primary cilia would induce AKT-Myc signaling activation

Gal8-induced primary cilia elongation was a drastic organelle morphological change within a short period of time. This event should elicit relevant physiological response in the MDCK cells. We analyzed total transcripts which pre-treated with PBS or His-Gal8 and recovery 5 hour with complete medium with Next Generation Sequencing (NGS). Compared to control cells, 3973 genes were identified as significantly changed (1932 were down-regulated; 2041 were up-regulated) in Gal8 pre-treatment cells. The gene sets analyzed with over-representation analysis (ORA) were significantly increased in Gal8 samples regulated cell proliferation pathways such as DNA replication, cell cycle mitotic, cell cycle checkpoint, Myc signaling, TGFβ signaling, and cell division (Fig.26A). In contrast, the gene sets which were significantly decreased in Gal8 samples are associated with cell adhesion signaling such as EGF signaling, TNF signaling, adipogenesis, extracellular structure organization, cilium organization, and cilium movement (Fig. 26B). There are given in the obtained heatmap (Fig. 26D) which indicated representative gene expression levels. Combined with the data from subsequent gene

doi:10.6342/NTU202302590

set analysis (GSEA), the hallmarker Myc target was significantly increased in Gal8 pre-treatment cells (Fig. 26C). Taken together, the ORA and GSEA implied that Myc signaling and cell replication programming should be activated after Gal8 binding to primary cilia. To verify the result from NGS, the EdU proliferation assay was used to investigate the effect of cell proliferation rate after Gal8 treatment (Fig. 27). The cell which was treated with PBS displayed a high level of cell proliferation activity. However, the EdU signal was significantly increased in Gal8 pre-treated cells. This result suggested that the ciliary Gal8 would promote DNA replication and cell proliferation. At protein level, Myc and phosphorylated AKT significantly increased after Gal8 treatment (Fig. 28). Taken together, our data implied that exogenous Gal8 binding to primary cilia TZ promoted primary cilia elongation. It was a hint to regulate AKT-Myc signaling activation and promote cell proliferation.

doi:10.6342/NTU202302590

DISCUSSION AND PROSPECTIVES

In this study, we demonstrated that apically secreted Gal8 binds to the primary cilia membrane and promotes primary cilia elongation in polarized epithelia. We also identified that the TZ of primary cilia is enriched with lipid raft component gangliosides and lipid raft scaffold protein, Cav1, which interact with Gal8. As primary cilia are elongated by extracellular Gal8, these lipid raft components as well as the TZ marker TMEM231 were translocated from the base of primary cilia into the axoneme These effects of extracellular Gal8 can be phenocopied by pharmacological inhibition of lipid raft and genetic ablation of Cav1. These results imply that the interaction between Gal8 and the TZ perturbs the function of TZ as a diffusion barrier to regulate molecular inflow and outflow of cilia axoneme.

Transition zone is a macromolecular complex located at the most proximal region of cilia axoneme, and immediately distal to the basal body [18, 19]. This residence of TZ at this region positions it as an ideal organelle to assume a role of a gate keeper to govern molecular inflow and outflow of the ciliary axoneme. In Caenorhabditis elegans genetic interaction studies, the TZ component genes have identified two major functional modules, Meckel syndrome (MKS) and Nephronophthisis (NPHP). If one or more gene(s) within one module are disrupted, ciliogenesis is mostly normal, although a subset of cilia are slightly shorter [60-62]. In stark contrast, deleting genes from both modules severely compromises ciliary structures [63, 64]. These findings imply that members of the MKS and NPHP modules can compensate each other's function in ciliogenesis. A third group of TZ proteins, for example, MKS-5 (RPGRIP1L/MKS5), act as an essential "scaffold" or "assembly factor" for most, if not all, MKS and NPHP module proteins [59, 65]. Given the drastic influence of exogenous Gal8 in ciliary morphology, it is likely that Gal8 can exert its effect on more than one of these TZ scaffold protein via caveolin 1. Our results

doi:10.6342/NTU202302590

confirm a previous study which reports a cilium-lengthening effect of knocking out caveolin 1α by gene editing approach [66]. The authors conclude that caveolin 1α activates RhoA and its downstream effectors, ROCK and DIA1, to regulate the apical actin meshwork, which affects the arrival of vesicles to the ciliary base, which subsequently affects cilium length. Caveolin-1 has also been reported to affect ciliary functions in sensory neuron of C. elegans by working together with endosome maturation factors rabenosyn-5/VPS45 to regulate ciliary membrane homeostasis [67].

Our data show that Gal8 played an important role in primary cilia elongation. However, the effect of gal8 depletion in cells is less explored in our study. In our previous research, we found that knockdown Gal8 causes abnormal lumen in the lateral domain and mislocalizes Gp135 during the polarization in MDCK cells [35]. Also, we observed that knockdown Gal8 decreased the ciliated cell number in polarized MDCK cells. With exogenous Gal8 treatment, it could promote primary cilia elongation but could not restore the number of ciliate cells. This result implied that Gal8 performs different functions in cytosol or extracellular space, respectively. In the study of Fátima Ferragut et al., they used lots of siRNA knockdown experiments that confirmed Gal8 depletion significantly affects cell adhesion and migration in breast cancer cells. Moreover, this study also indicates that cell sialylation is important in Gal8-mediated cell adhesion [68]. This is consistent with our conclusion that the substrates with negative charge were the interacting target of Gal8.

In this study, we showed that the frequency of the cells with a primary cilium was diminished by Gal8 knockdown while extracellular Gal8 elicited cilial elongation. This implies Gal8 behaves as an autocrine/paracrine factor to modulate epithelial morphogenesis. It is generally accepted that galectins, which lack the signal sequence for classical secretory pathway, are sent to extracellular space through unconventional protein transportation [52]. Both exosomes and ectosomes are

doi:10.6342/NTU202302590

extracellular vesicles which allow cells to release bioactive molecules independent of the classical secretory pathway [69]. We favor ectosomes over exosomes as the transportation machinery of apically secreted Gal8 because there are quite a few number of Gal8 interacting partners identified by our proteomic approach (Table 1) which are also confirmed ectosome components such as integrins [70, 71] LAMP1 [72], flotilin 1 [73], and ezrin [74, 75].

Although those proteins dependent on unconventional routes for their secretion do not share obvious common motifs or features in their sequence or structure, most unconventionally secreted proteins are reported to bind phospholipids. Indeed, anoctamin-6 (ANO6, also known as TMEM16F) is a lipid scramblase that has been demonstrated to facilitate the translocation of annexins, which are known to bind to negatively charged lipid and be secreted through unconventional pathways, across plasma membrane [76]. Intriguingly, annexin A1 and anoctamin-6 were both identified in this study as the apical interactome candidates for extracellular Gal8 (Fig. 19 and Table 1). Given that anoctamin is expressed at the primary cilia in polarized MDCK monolayer [77] and our study reveals Gal8 interacted with the lipid raft components, it would be interesting to explore whether anoctamin plays a role in the location of Gal8 at primary cilia and the cilia-lengthening effects of Gal8.

Another interesting finding revealed by our apical interactome screening for Gal8 comes from the identification of several ATP binding cassette (ABC) transporters (Fig. 19 and Table 1). Although ABC family transporters have not been reported to be involved in export of galectins, ATP binding cassette A1 (ABCA1) transporter is implicated in the secretion of annexin A1, another membrane lipid binding protein which also lacks leader peptide signal as galectin [78, 79]. Furthermore, it has been demonstrated in murine leukocytes that the P4-type ATPase ATP11C possesses significant flippase activity [80]. Whether lipid scramblases such as anoctamin 6 or any ABC transporter facilitates the unconventional secretory process of galectins

doi:10.6342/NTU202302590

is an interesting issue awaits further investigation.

Our transcriptomic analysis disclosed that several genes related to cell replication and cell cycle process were up-regulated (Fig, 26A and 26B). The GSEA analysis exhibited similar results and myc signaling pathway has been up-regulated after Gal8 treatment (Fig. 26C). In conjunction with the mass spectrometry, we noted that Gal8 has strongly interacted with the receptor tyrosine kinase, IGF1R, of the MDCK cell apical domain (Table 1). At the protein level, the AKT which was a downstream target of IGF1R and a well-known cell survival/proliferation factor [81] was activated (Fig. 28). At primary cilia, IGF1R, receptor tyrosine kinases, localize on the cilia membrane and transmit the signaling after ligand stimulation to activate downstream signaling, such as phosphoinositide 3 kinase (PI3K)/AKT signal, at the primary cilia base [82, 83]. Primary cilia base content basal body, distal/subdistal appendages, and special membrane area which is Phosphatidylinositol 4, 5-bisphosphate ($PI(4,5)P_2$) enrich region [84]. The classic PI3K-AKT signaling is activated PI3K phosphorylate $PI(4,5)P_2$ to $PI(3,4,5)P_3$ then phosphorylate AKT and turn on the downstream signaling transduction [85]. Taken together, our study found that Gal8 would interact with IGF1R to activate downstream AKT at the cilia base and then activated Myc through inhibited GSK3β. Thus, it is likely that Gal8 binding to primary cilia promotes the cell cycle progression.

doi:10.6342/NTU202302590

FIGURES

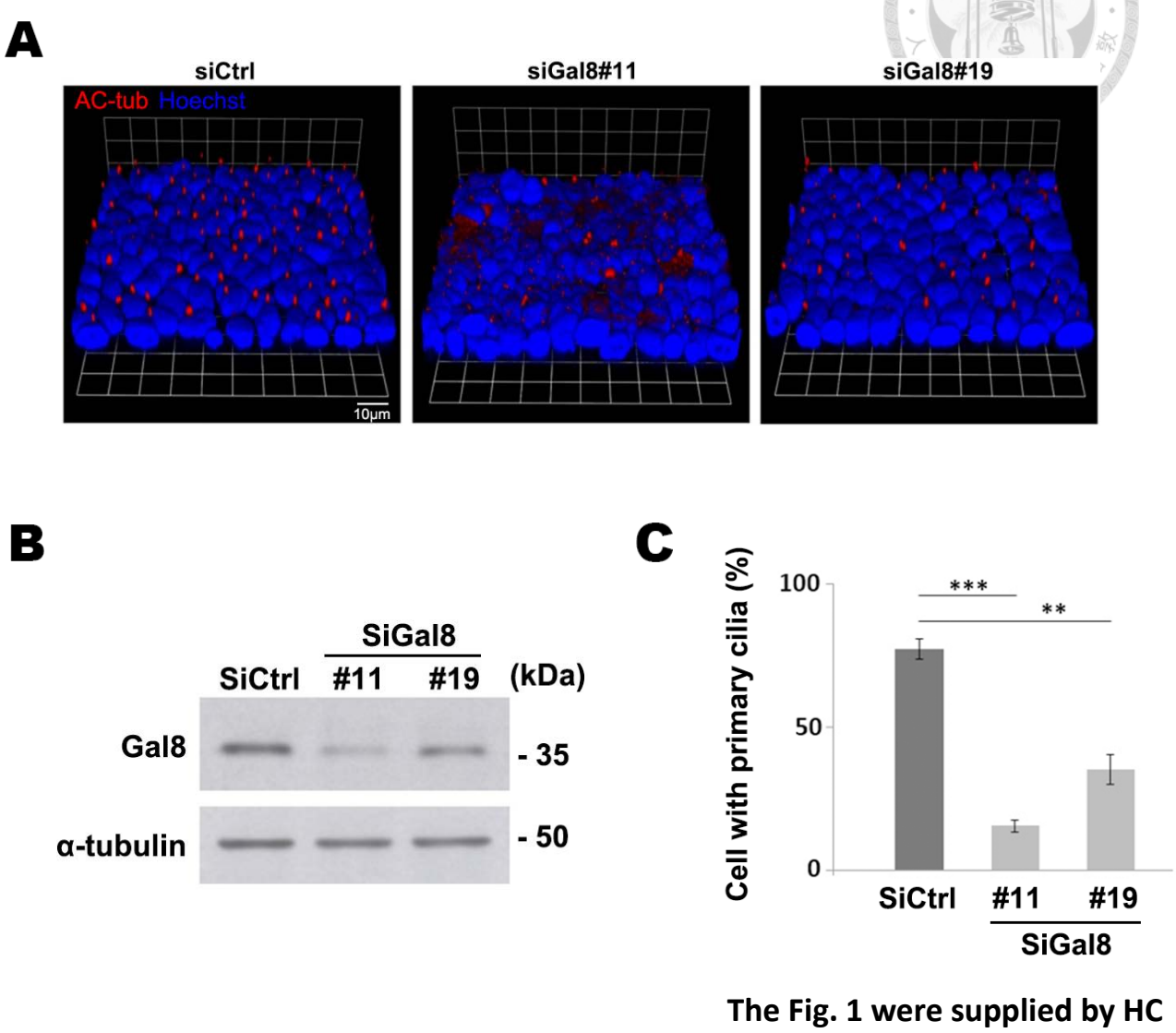

The Fig. 1 were supplied by HC

Fig. 1 Knockdown endogenous Gal8 reduced ciliogenesis.

(A) The confocal images showed the pattern of primary cilia in siGal8 stable clones and mock control on MDCK cell apical domain. (B) Western blot showed efficient down-regulation of endogenous Gal8 expression in two independent MDCK stable clones expressing shRNA targeted at galectin 8 as compared to the mock control. (C) Morphometric analysis quantifying the extent of ciliogenesis (bar chart was depicted for means and standard deviations (SDs), n > 200, $^{**}P < 0.01$, $^{***}P < 0.001$) and representative immunofluorescence images (left) in these cells.

doi:10.6342/NTU202302590

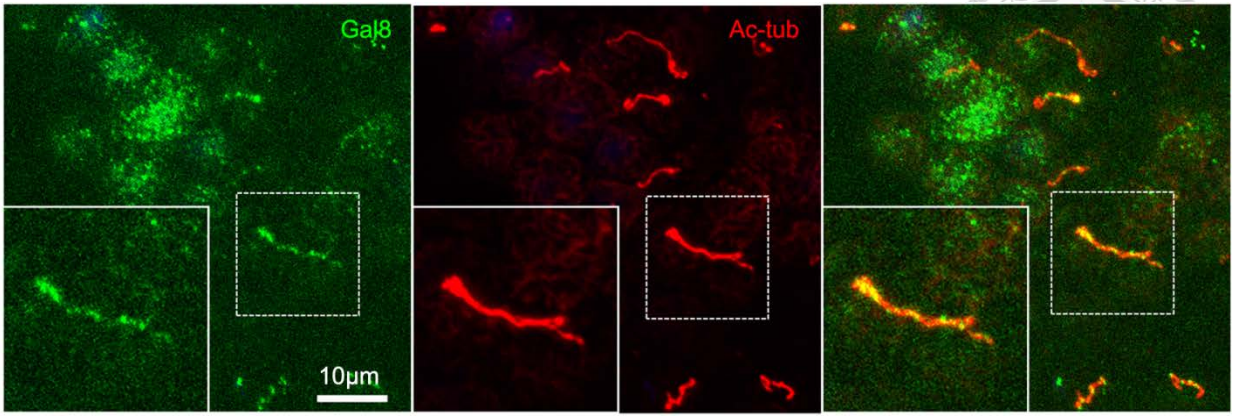

The Fig. 2 was supplied by HC

Fig. 2 Endogenous Gal8 was localized on primary cilia.

Polarized MDCK cells were processed for immunofluorescence using mouse anti-acetylated tubulin and rabbit anti-galectin 8 antibodies.

doi:10.6342/NTU202302590

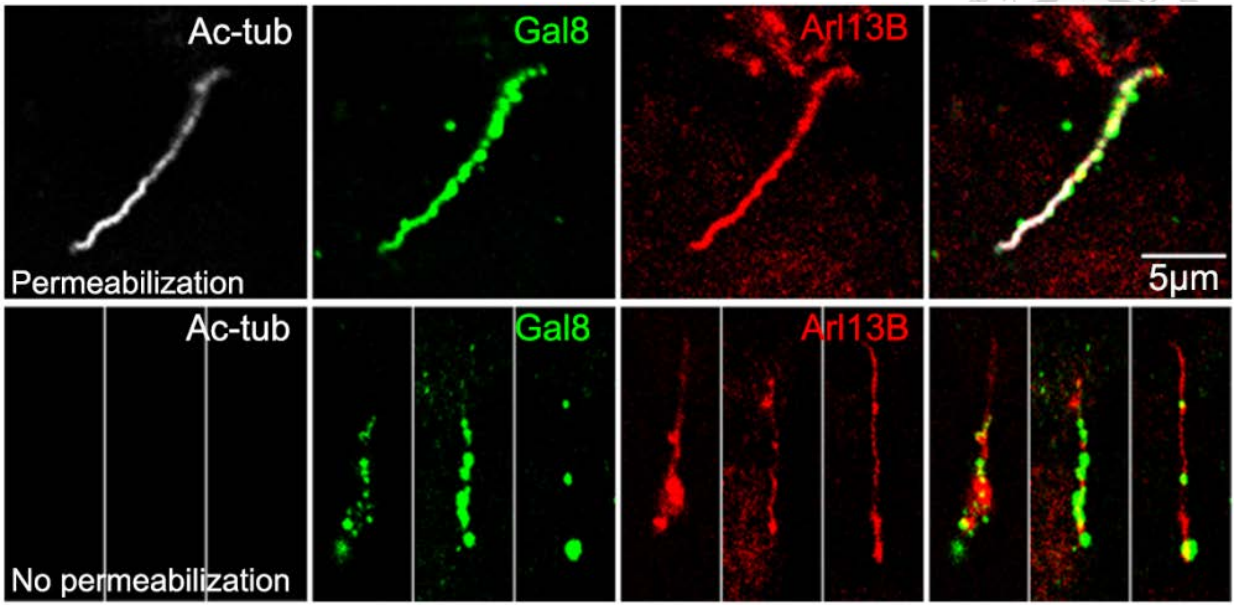

Fig. 3 Extracellular Gal8 interacted with primary cilia membrane.

Confocal images showing the patterns of endogenous Gal8 (green) and the primary cilia marker-acetylated tubulin (white) in a MDCK cell line stably expressing mCherry-tagged Arl13B which were either fixed and permeabilized (upper) or only fixed but not be permeabilized (lower) before procession for double immunostainings.

doi:10.6342/NTU202302590

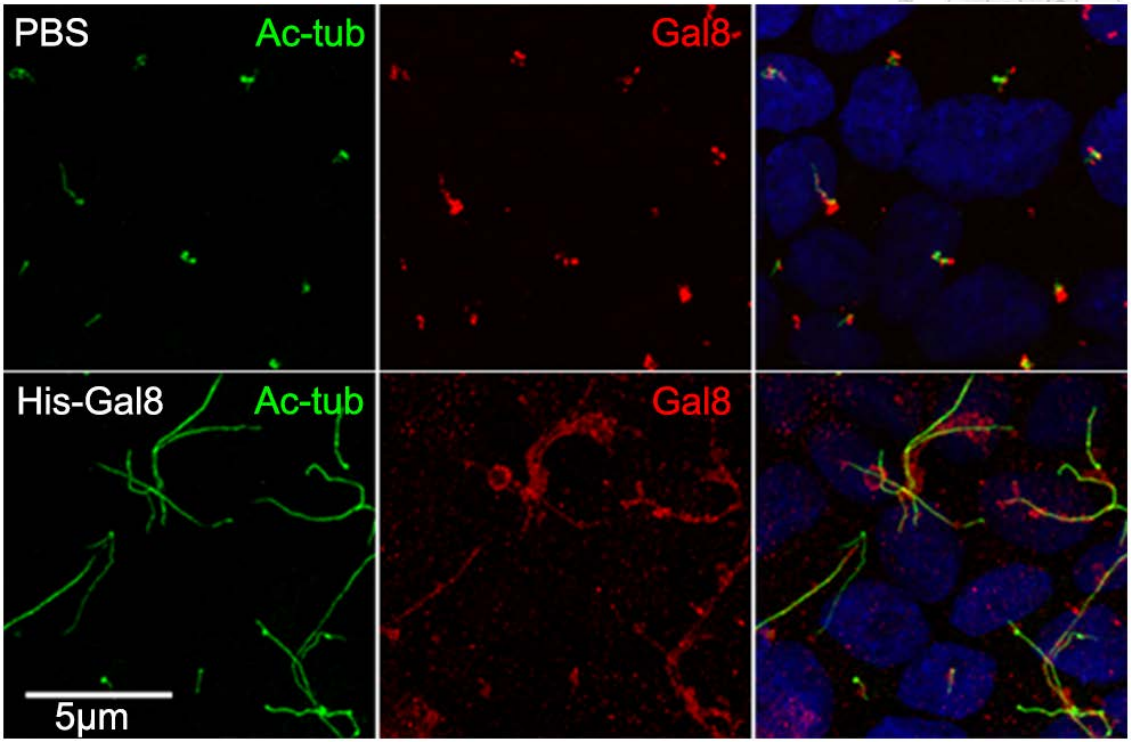

Fig. 4 Extracellular Gal8 interacted with primary cilia membrane and regulated ciliogenesis.

Double immunofluorescence study in polarized MDCK cells revealed that exogenous His-Gal8 (0.1 μg/μl) added on apical domain elicited primary cilia lengthening compared with PBS treatment.

doi:10.6342/NTU202302590

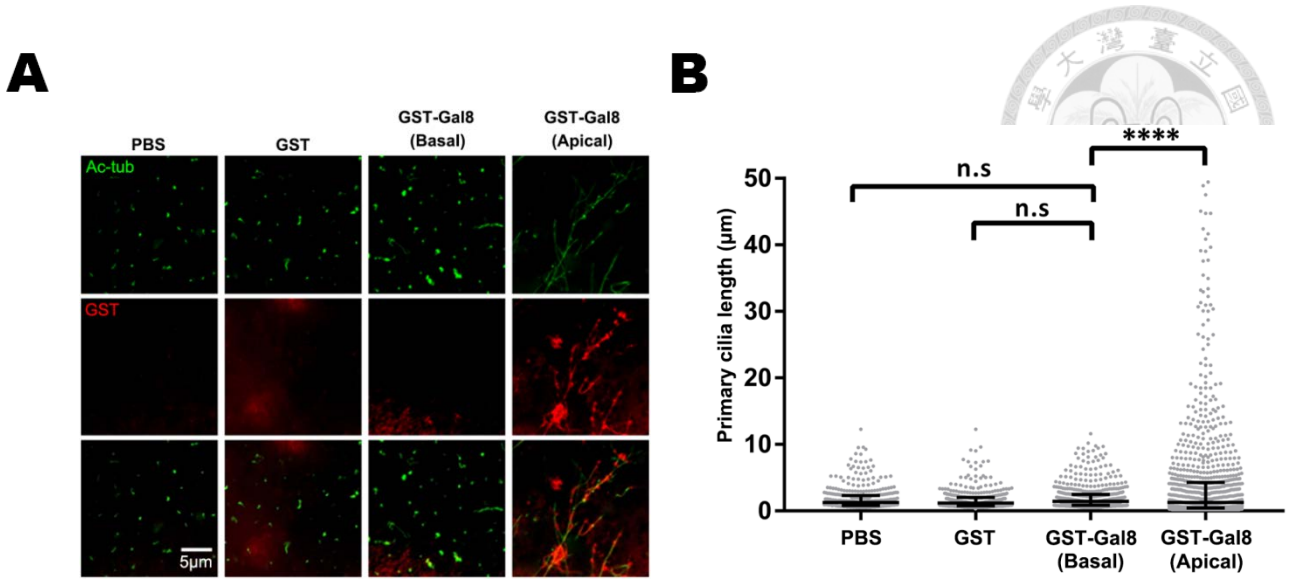

Fig. 5 Extracellular Gal8 interacted with primary cilia membrane on apical domain.

(A) Exogenous GST-Gal8 (0.2 μg/μl) treatment onto apical domain of polarized MDCK monolayer promoted primary cilia elongation, but no effect was observed when the recombinant protein was applied onto basolateral domain. (B) Quantification of primary cilia length for the study presented in (A). Data were showing the lengths of primary cilia in individual cells from 3 independent experiments. The median with interquartile range of experiments were shown as black bars. The statistical significance was calculated by Kruskal–Wallis with Dunn's test. n > 200, not significant (n.s.) $P > 0.05$, ****$P < 0.0001$.

doi:10.6342/NTU202302590

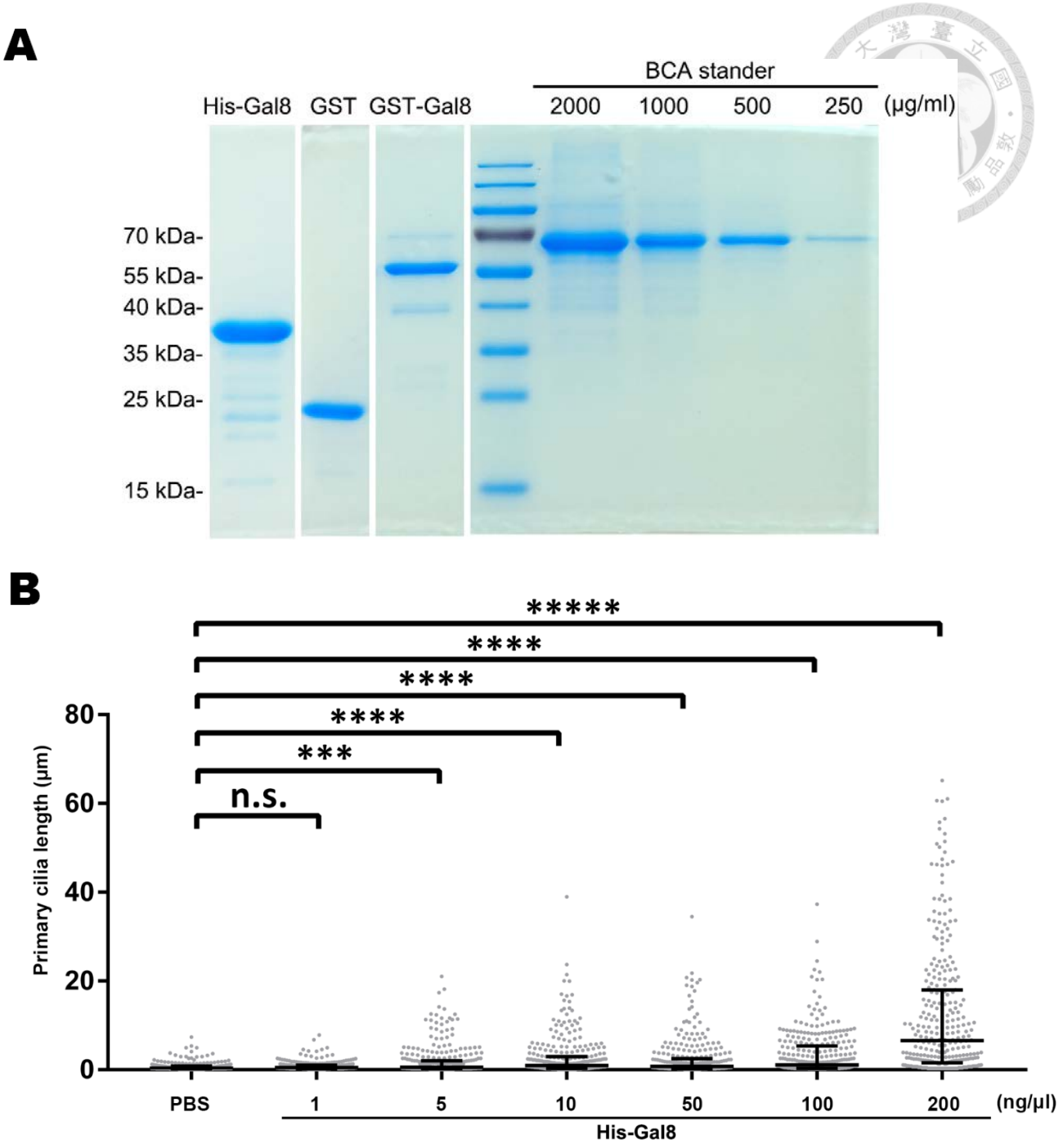

Fig. 6 Recombinant Gal8 facilitated primary cilia lengthening in a dose-dependent manner. (A) The purification of His tag or GST tag galectin 8 and GST-only recombinant proteins were stained with coomassie blue. (B)Polarized MDCK epithelia were added with the indicated concentration of His-Gal8 from the apical surface for 30 min before the length of primary cilia was quantified by immunofluorescence study using acetylated tubulin staining. Data were quantified with nonparametric test. n > 200, n.s. P > 0.05, ***P < 0.001, ****P < 0.0001.

doi:10.6342/NTU202302590

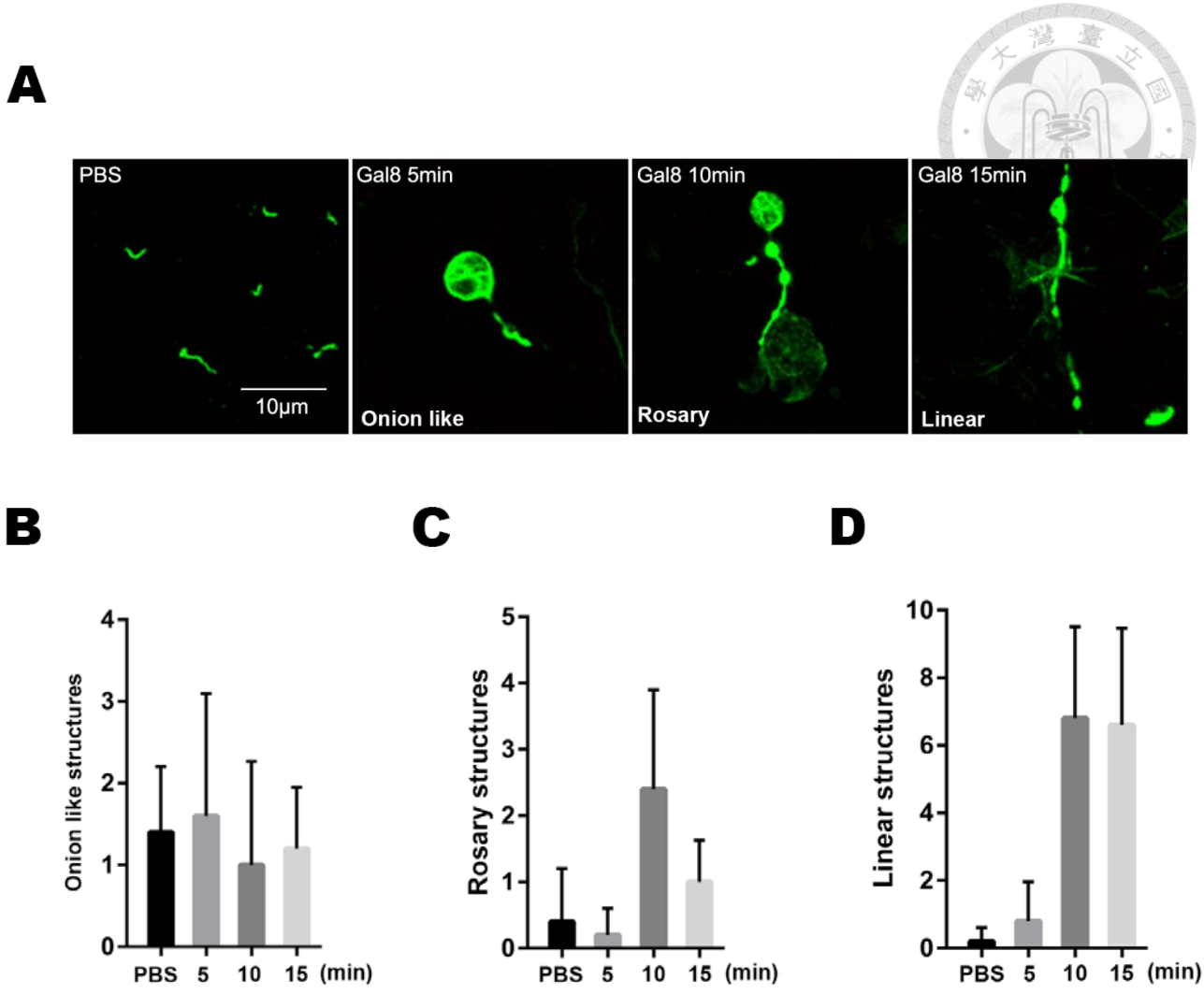

Fig. 7 Recombinant Gal8 facilitated primary cilia lengthening through transient intermediate tubulin based structures.

(A) Polarized MDCK epithelia were added apically with His-Gal8 (0.1 μg/μl) for the indicated time before the cells were processed by immunostaining using antibody recognizing acetylated tubulin. The numbers of three distinct cilia-related structures were measured within 5 randomly selected microscopic fields at each time point. Data were expressed as mean bars and SDs. The numbers of onion like (B), rosary (C), and linear (D) structures were quantified at the indicated time points after His-Gal8 treatment.

doi:10.6342/NTU202302590

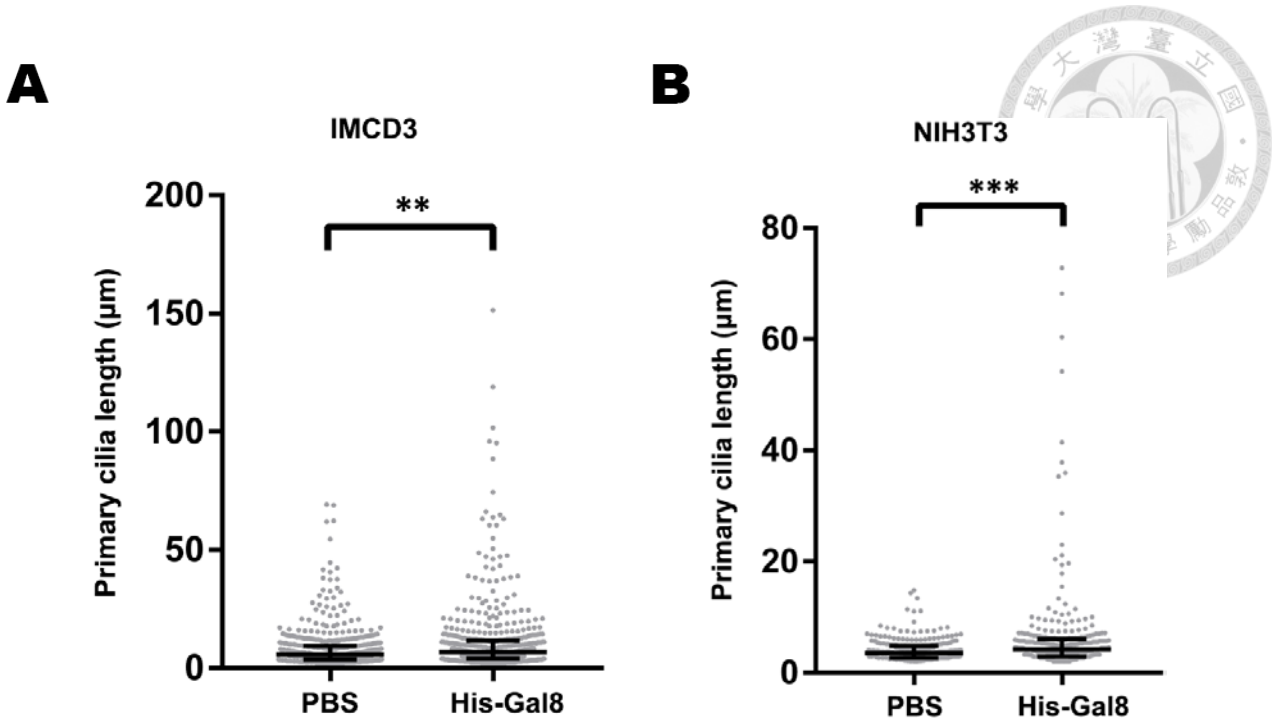

Fig. 8 Recombinant Gal8 facilitated primary cilia lengthening in NIH3T3 and IMCD3 cells. (A) NIH3T3 fibroblasts and (B) IMCD cells were treated with His-Gal8 (0.1 μg/μl) for 30 min before the length of primary cilia was quantified by immunofluorescence study using acetylated tubulin staining. Data were quantified with nonparametric test. n > 200, **P < 0.01, ***P < 0.001.

doi:10.6342/NTU202302590

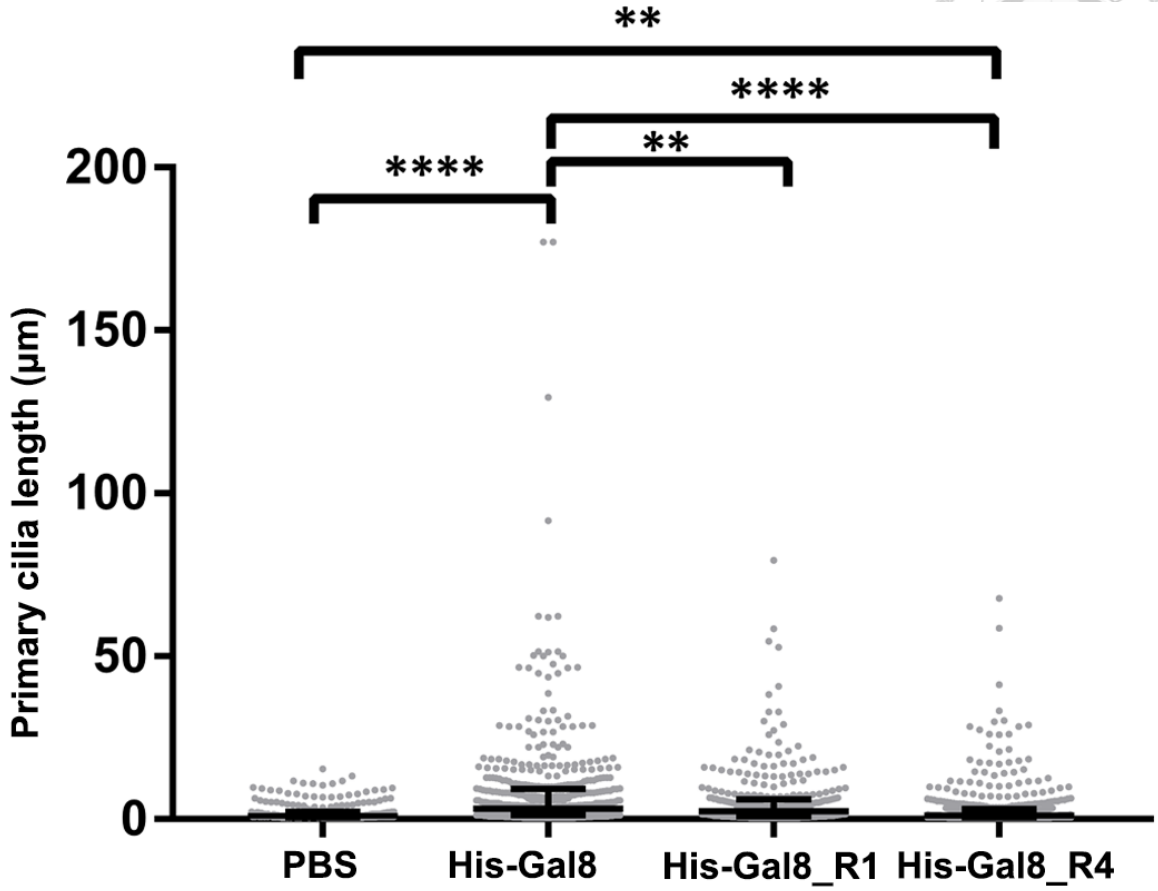

Fig. 9 Primary cilia resorption followed after recombinant Gal8 was removed.
Polarized MDCK epithelia were added apically with His-Gal8 (0.1 μg/μl) for 30 min followed by recovery in complete medium for 1 (His-Gal8_R1) or 4 (His-Gal8_R4) h before the cells were processed by immunostaining using antibody recognizing acetylated tubulin. Data were quantified with nonparametric test. n > 200, **P < 0.01, ****P < 0.0001.

doi:10.6342/NTU202302590

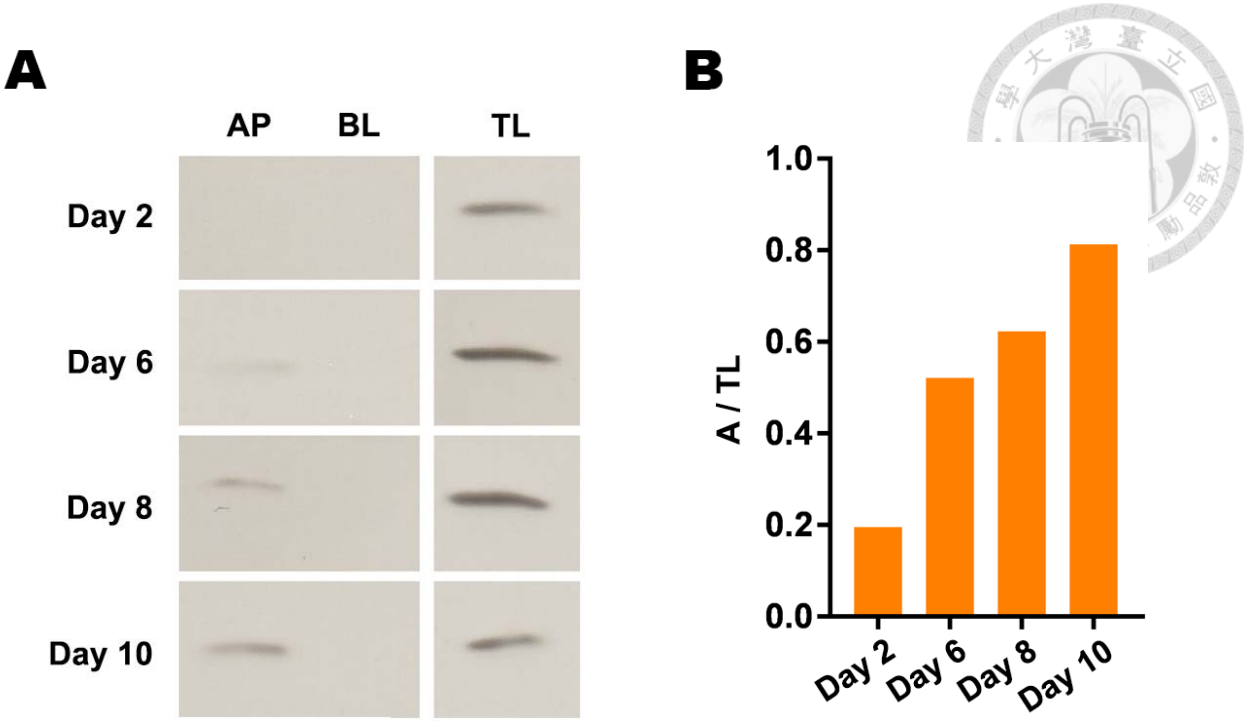

Fig. 10 Gal8 was secreted to apical domain during epithelial polarization.

(A) Culture media were collected from apical (AP) and basolateral (BL) compartments of FLAG-tagged Gal8 stably expressing MDCK cells grown on Transwell for the indicated periods. These conditioned media were immunoprecipitated with mouse anti-FLAG antibody before being processed for SDS-PAGE together with 10% of total cell lysates (TL) and analyzed by Western blot analysis using mouse anti-FLAG antibody. (B) Quantification of AP/TL ratio in (A)

doi:10.6342/NTU202302590

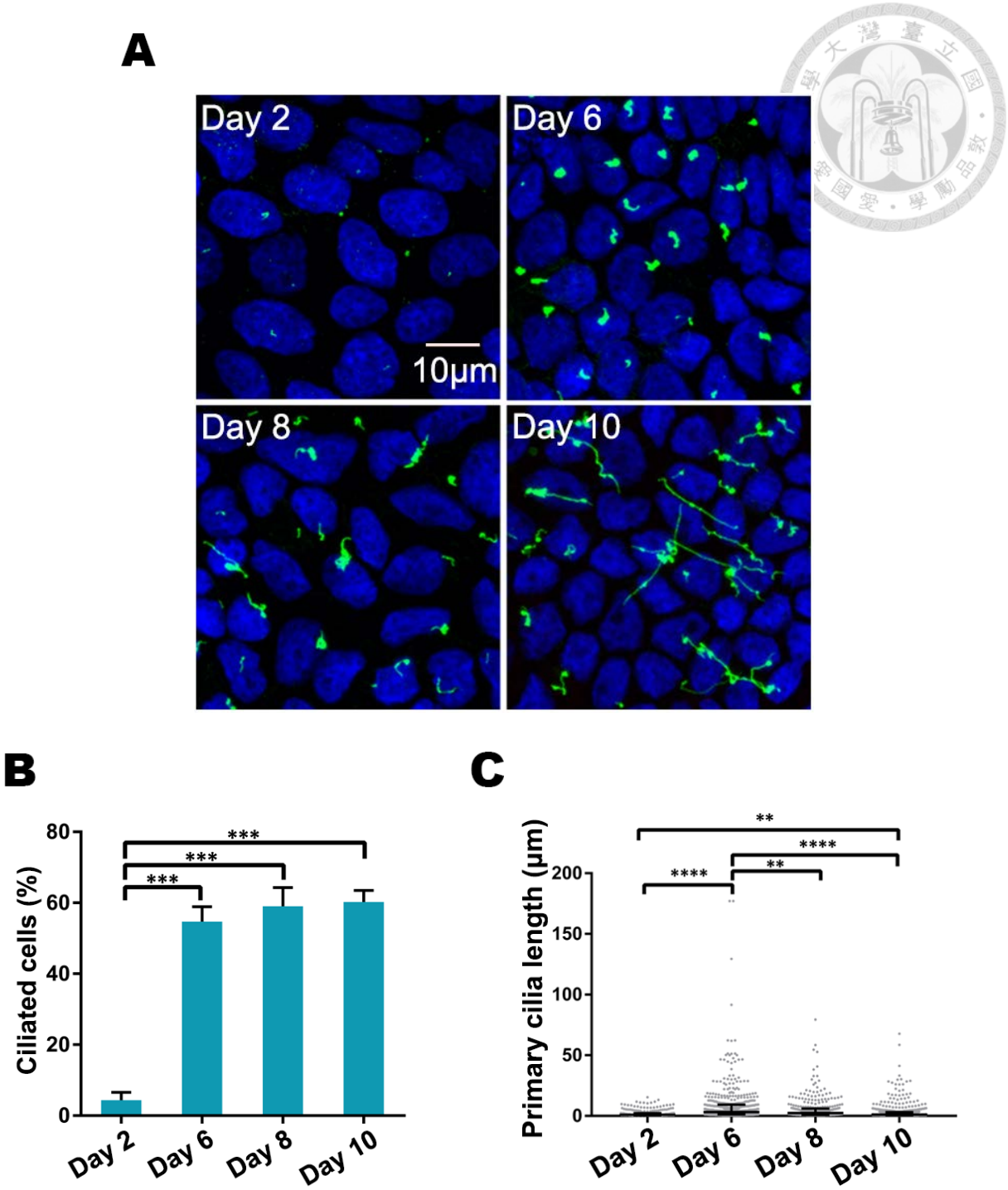

Fig. 11 Both the primary cilia length and the number of ciliated cells increased during epithelial polarization.

(A-C) MDCK cells were grown on Transwell for the indicated periods and processed for immunostaining for acetylated tubulin and Hoechst staining to quantify the percentage of (B) ciliated cells (data were expressed as means and SDs, n > 200, ***P < 0.001 as compared to day 2) and (C) average primary cilia length (individual measurements were quantified with nonparametric test. n > 200, **P < 0.01, ***P < 0.001 as compared to day 2).

doi:10.6342/NTU202302590

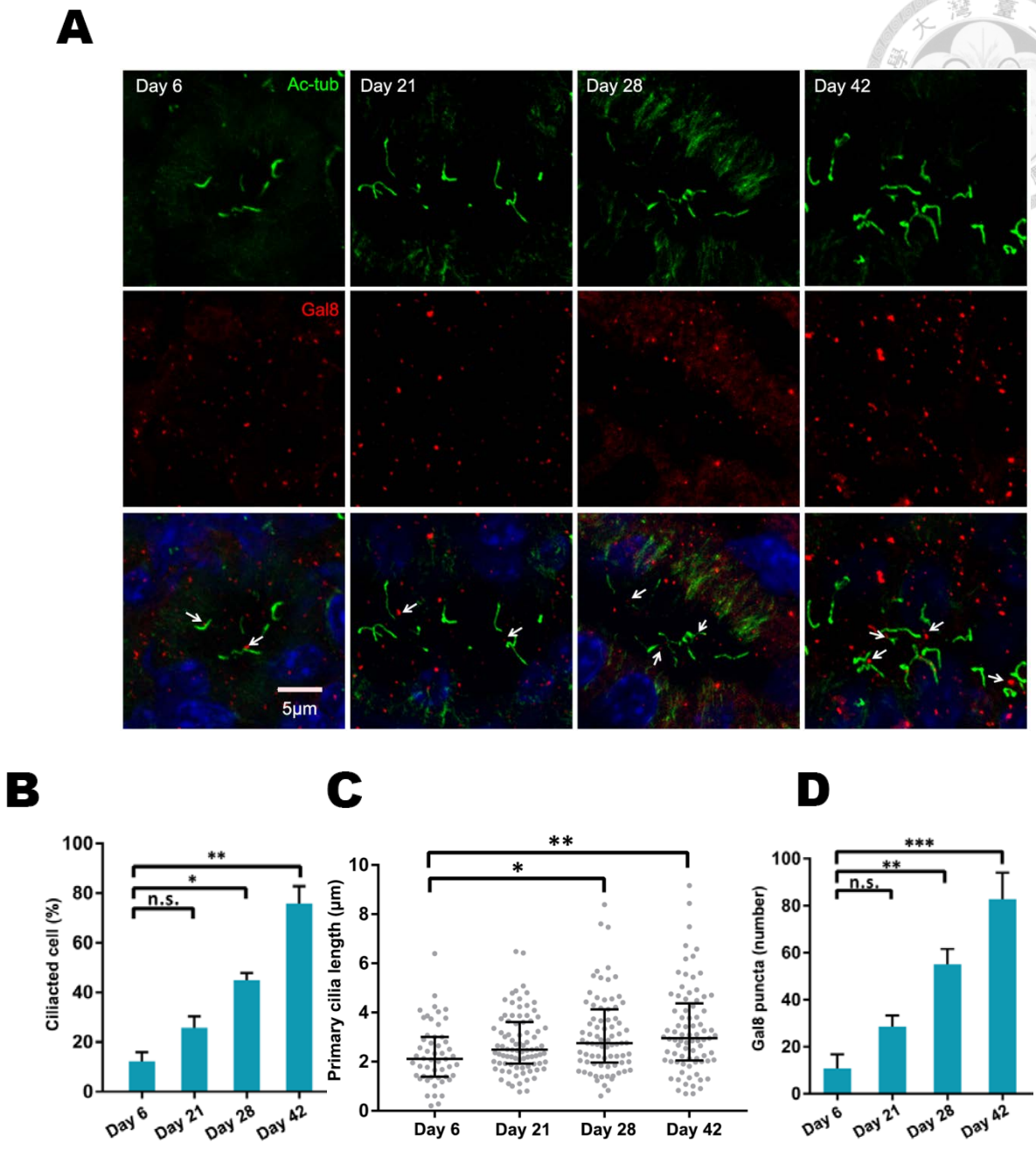

Fig. 12 Gal8 was secreted to the apical domain during mouse kidney development.

(A) Kidney tissue sections were prepared from mice of the indicated postnatal ages and processed for immunofluorescence using mouse anti-acetylated tubulin and rabbit anti-galectin 8 antibodies. White arrowheads indicated where galectin 8 was found near the bases of lengthy primary cilia. (B) Quantification of ciliated cells , (C) the length of primary cilia , and (D) the number of galectin 8 puncta in renal tubular epithelia from mice of the indicated postnatal ages. Data were expressed as median with interquartile range in bar chart and quantified with nonparametric test, n > 50, n.s. P > 0.05, *P < 0.05, **P < 0.01 as compared to day 6.

doi:10.6342/NTU202302590

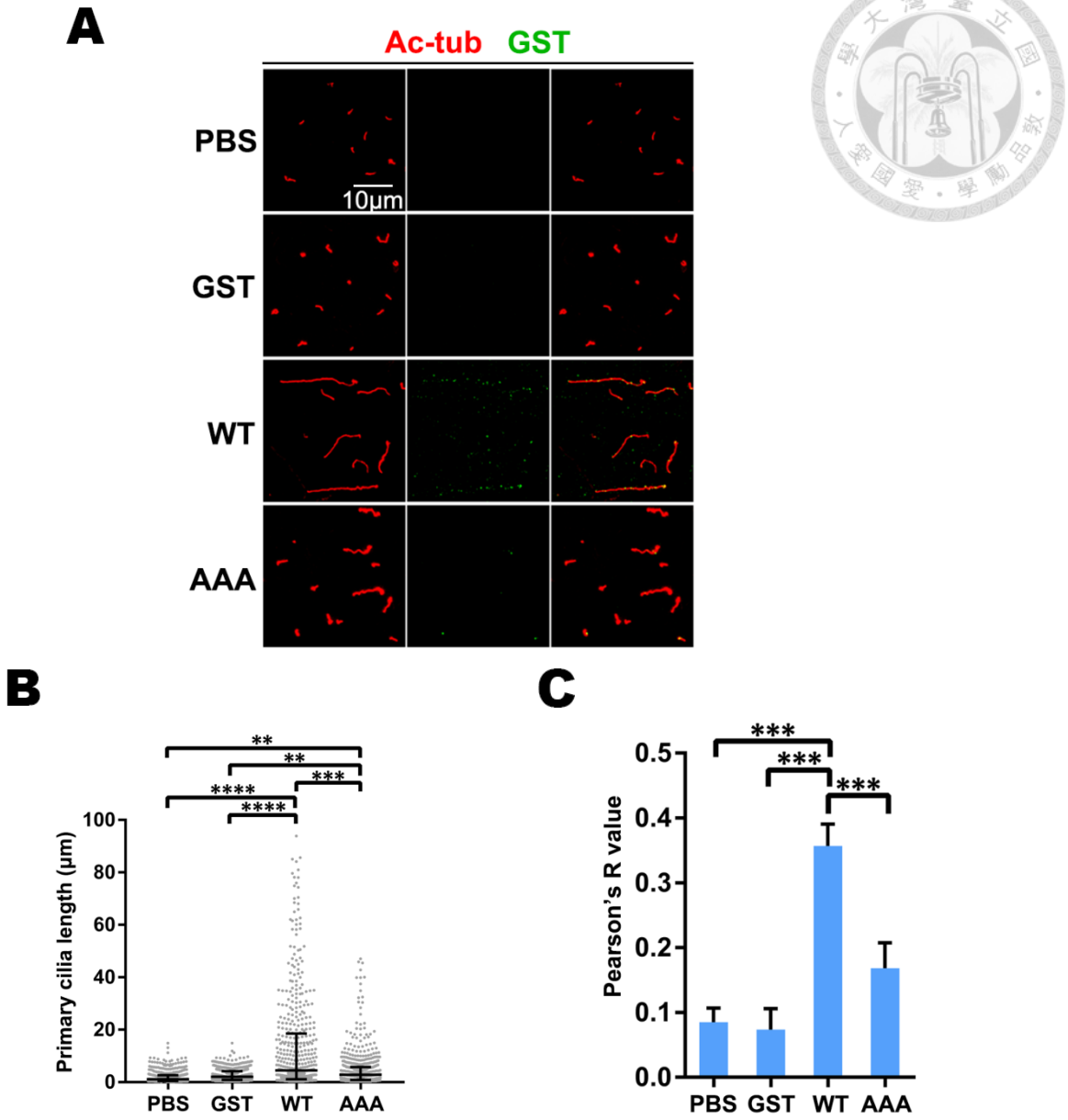

Fig. 13 Gal8 interacted with the primary cilia and this interaction contributed to the cilia-elongating effect of Gal8.

(A) Purified recombinant GST-Gal8 or the sialic acid binding defective mutant GST-Gal8-AAA protein (0.2 μg/μl) was applied onto apical domain of polarized MDCK monolayer at 4°C for 30 min, respectively. After extensive washing, immunofluorescence staining with mouse anti-acetylated tubulin and rabbit anti-GST antibodies was used to assess the extents of these recombinant proteins retained on the surfaces of primary cilia. Both (B) primary cilia length and (C) colocalization of the Gal8 recombinant proteins with the cilial marker acetylated tubulin were quantified. The data were quantified with nonparametric test, and the median with interquartile range were shown as black bars, n > 200, ***P < 0.001.

doi:10.6342/NTU202302590

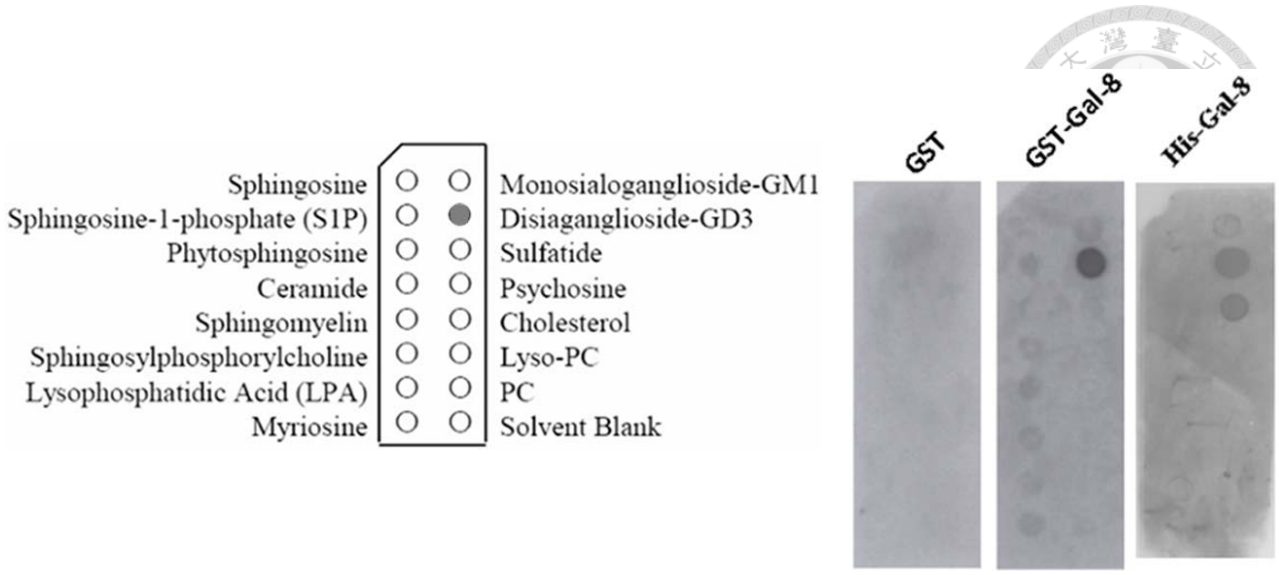

Fig. 14 Recombinant Gal8 specifically interacted with ganglioside-GD3.

The potential interaction between sphingolipid and Gal8 was evaluated by incubation of a commercial sphingolipid strip with GST, GST-Gal8, or His-Gal8, respectively. After extensive washing, the bound recombinant proteins were revealed by immunoblotting analysis with GST or His antibodies.

doi:10.6342/NTU202302590

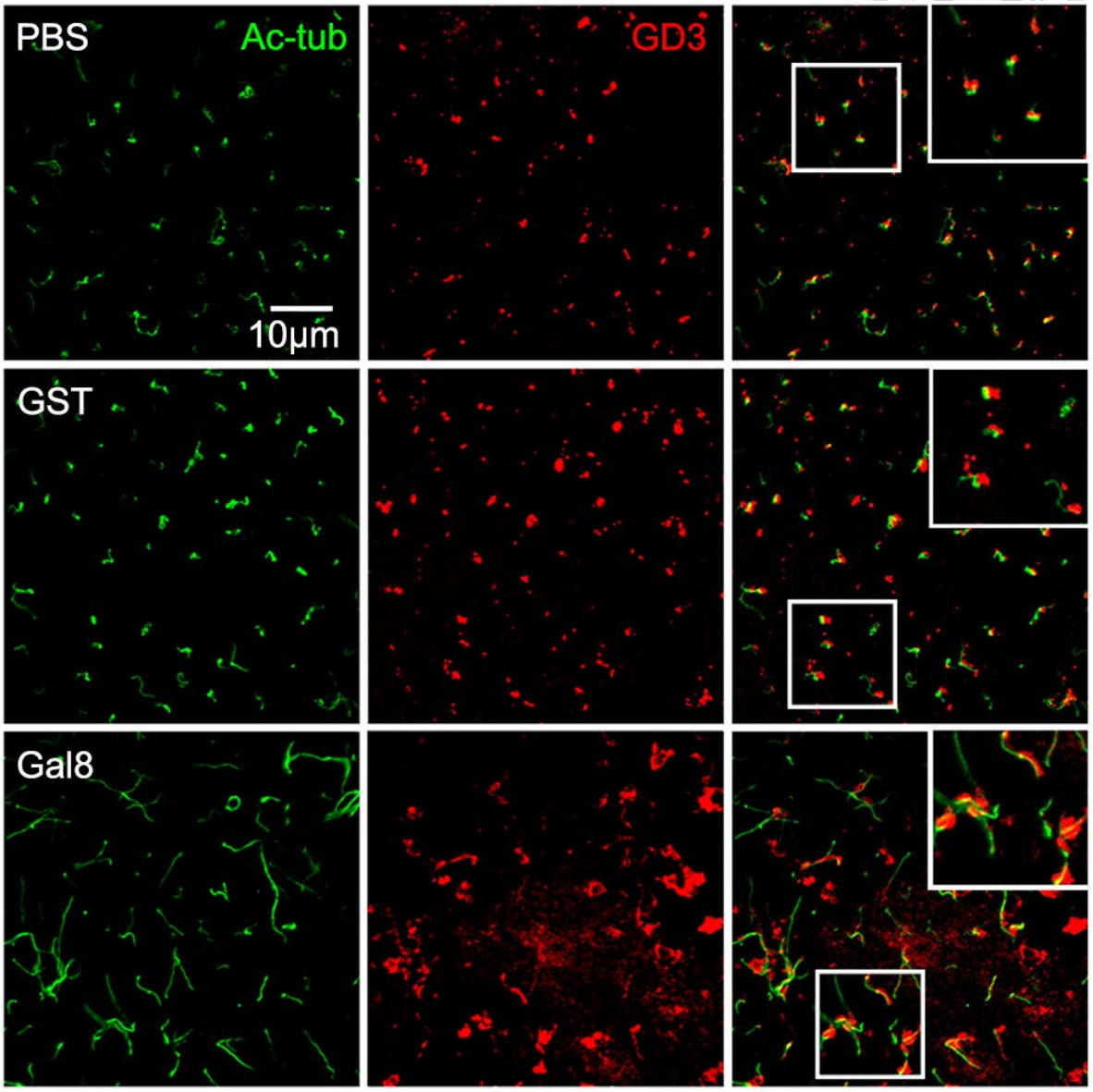

Fig. 15 Ganglioside-GD3 was localized on the primary cilia base.

Polarized MDCK cells were treated with PBS, GST, or GST-Gal8 (0.2 μg/μl), respectively, and processed for double immunofluorescence study with rabbit anti-acetylated tubulin and mouse anti-GD3 antibodies. The inserts in the overlapped channels showed the details of the spatial relationship between GD3 and cilia within the boxed areas.

doi:10.6342/NTU202302590

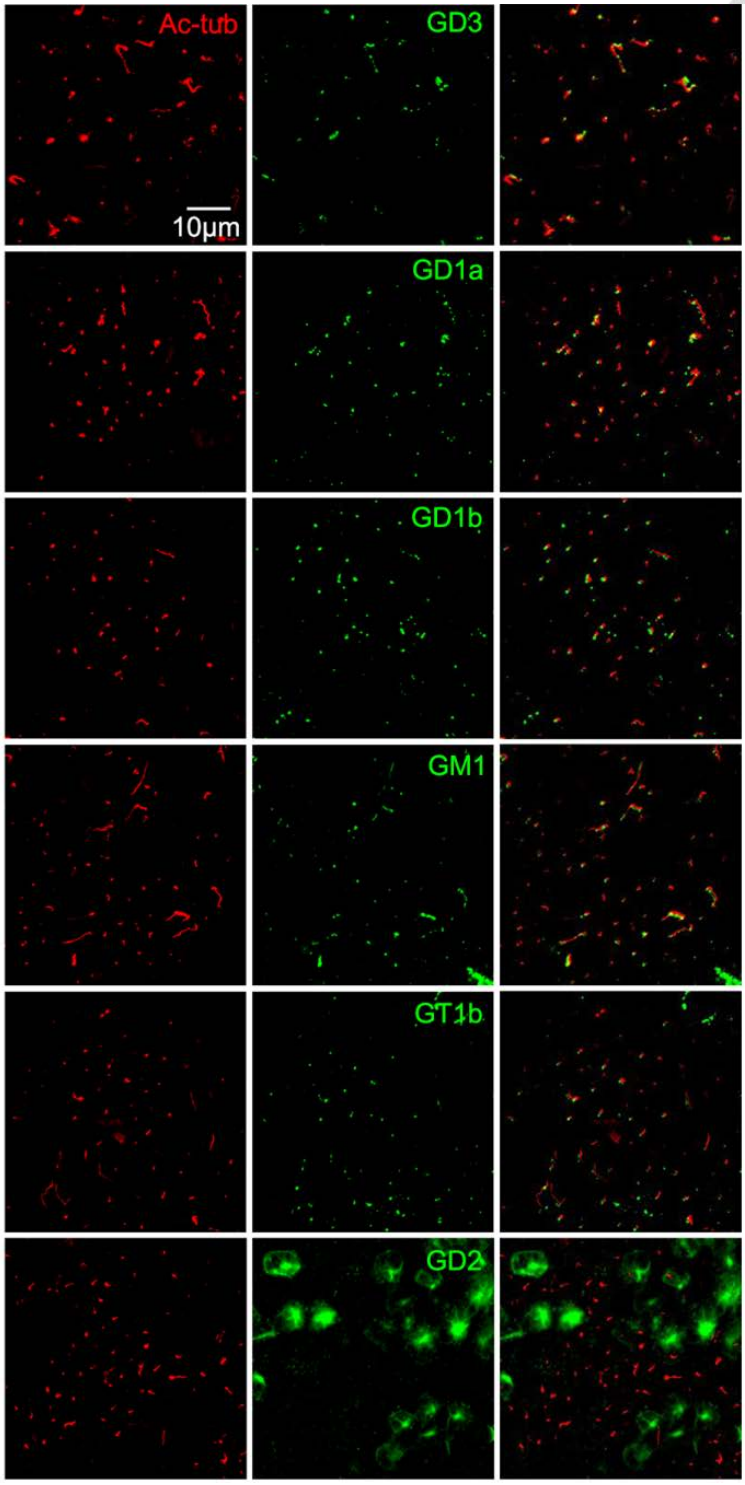

Fig. 16 Several gangliosides were localized on the primary cilia.

Polarized MDCK cells were processed for immunofluorescence using rabbit anti-acetylated tubulin and the indicated ganglioside specific mouse antibodies.

doi:10.6342/NTU202302590

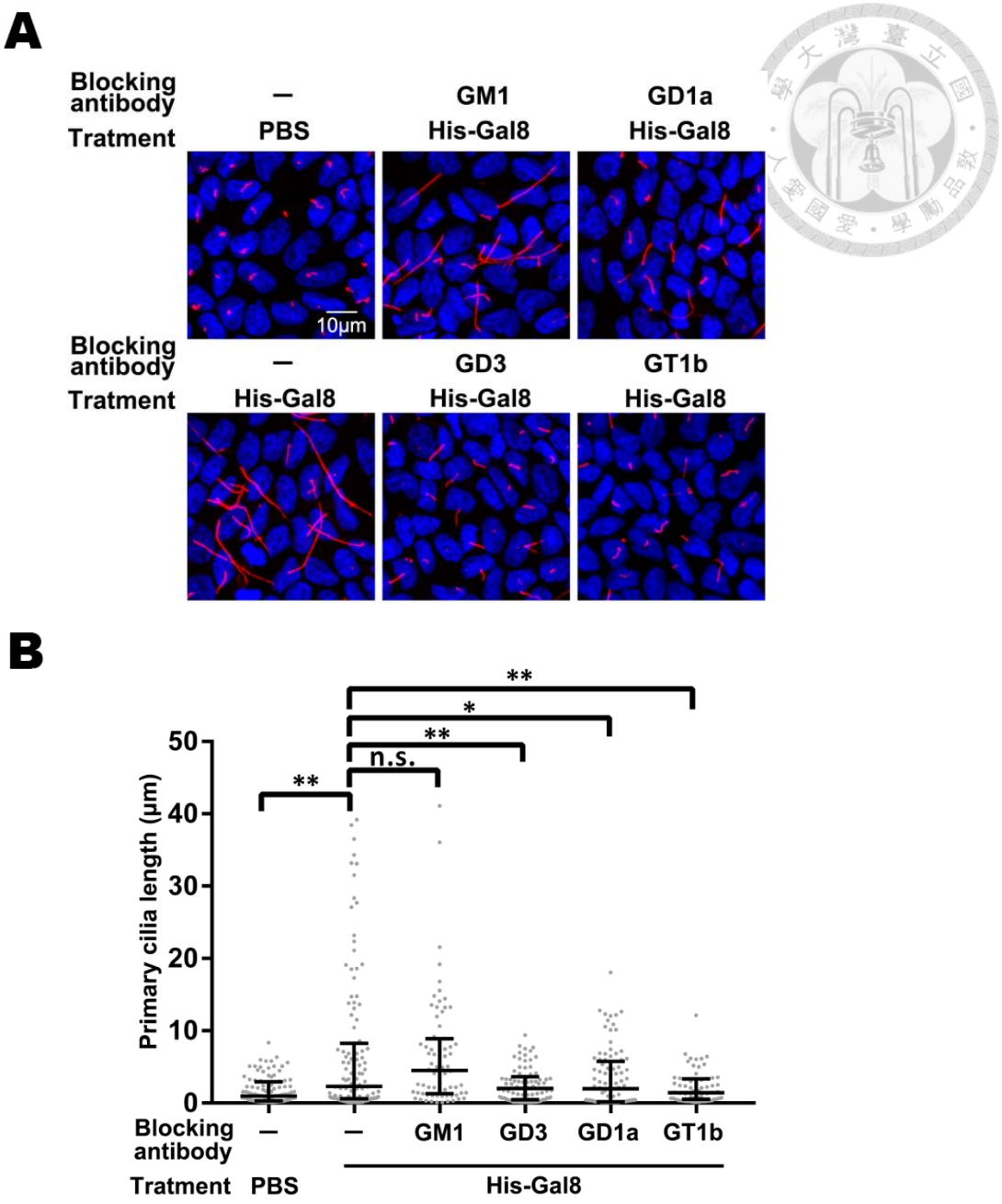

Fig. 17 Gal8 interacted with gangliosides on the primary cilia and this interaction contributed to the cilia-elongating effect of Gal8.

(A) MDCK cells were seeded onto Transwell. After fully polarization, the MDCK monolayers were blocked with the indicated ganglioside antibodies added onto the apical domain for 1 h on ice. Afterwards, the unbound antibodies were washed off at 4°C before the cells were incubated with purified GST-Gal8 applied into the apical compartment. (B) Quantification of primary cilia length was assessed by immunofluorescence staining using anti-acetylated tubulin antibody. The data were quantified with nonparametric test, n > 200, n.s. $P > 0.05$, *$P < 0.05$; **$P < 0.01$. f Representative confocal images from the study described in (e).

doi:10.6342/NTU202302590

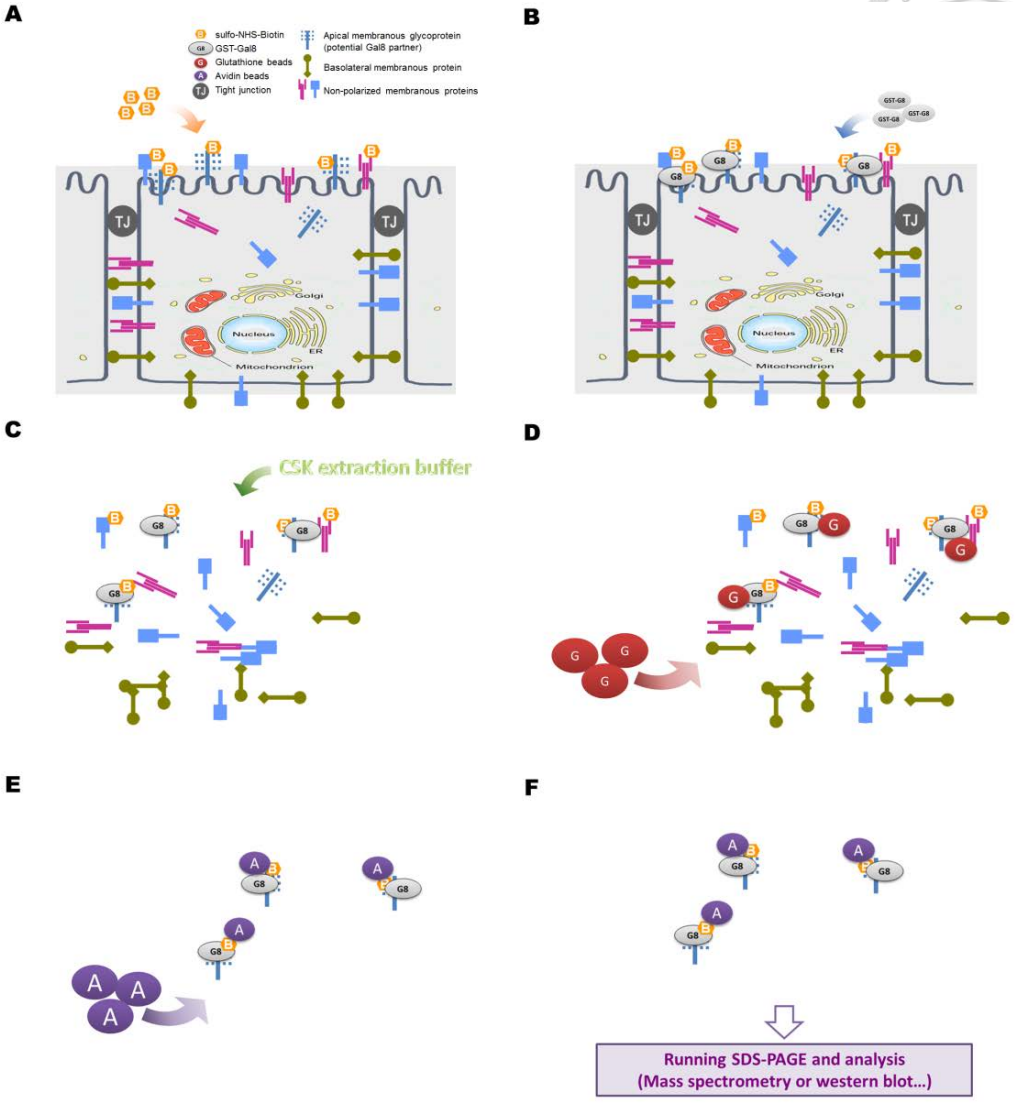

Fig. 18. Scheme of the strategy used to identify apical interactome for galectin 8.

Polarized MDCK cells grown on Transwell were apically biotinylated using plasma membrane-impermeable sulfo-NHS biotin at 4°C for 1 h (this was to limit the conjugation of the biotin with free amino group specifically at the exo-leaflet of apical membrane) followed by quenching the un-reacted biotin. GST-Gal8 was then incubated at 4°C for another 1 h. After washing off the un-bound recombinant GST-Gal8 protein, we then extracted the cells and applied these lysates onto glutathione beads for pulling down the recombinant GST-Gal8 and its interacting proteins. After careful washing, we then eluted GST-Gal8 and its binding partners from the beads using high concentration of free competing glutathione. Then, we bound the eluent with streptavidin beads. After overnight binding, we washed in high stringency condition, and then separated the remaining materials by SDS-PAGE. We then processed the samples for liquid chromatography and mass spectrometry to identify the apical interactome of Gal8.

doi:10.6342/NTU202302590

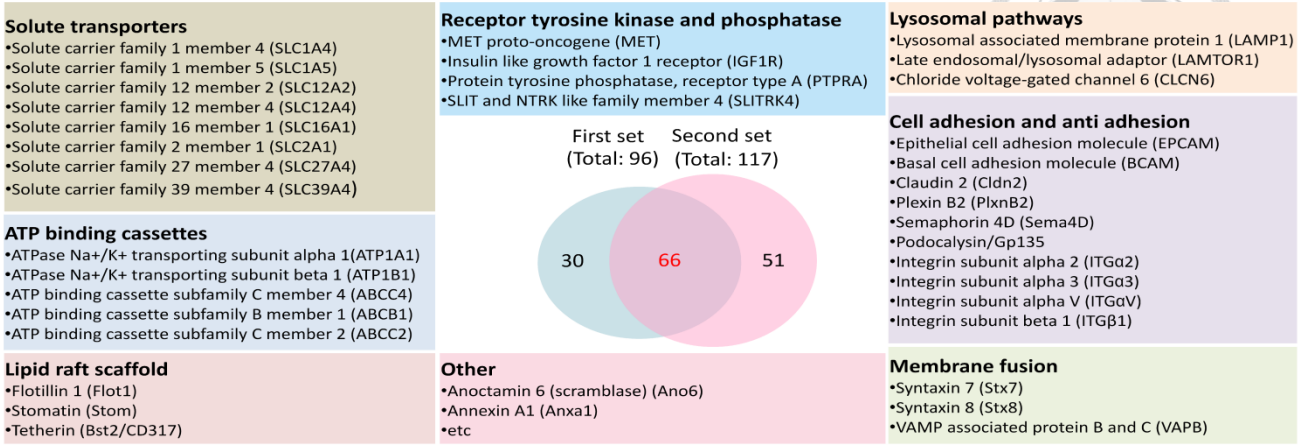

Fig. 19 The apical Gal8-interacting plasma membrane candidates were identified by mass spectrometry analysis.

Venn diagram indicating the two sets of membrane proteins that were identified by two independent mass spectrometry analyses, respectively. Totally 66 candidates (complete information was shown in Table S1) were identified by both analyses and were further categorized by their functional characterization.

doi:10.6342/NTU202302590

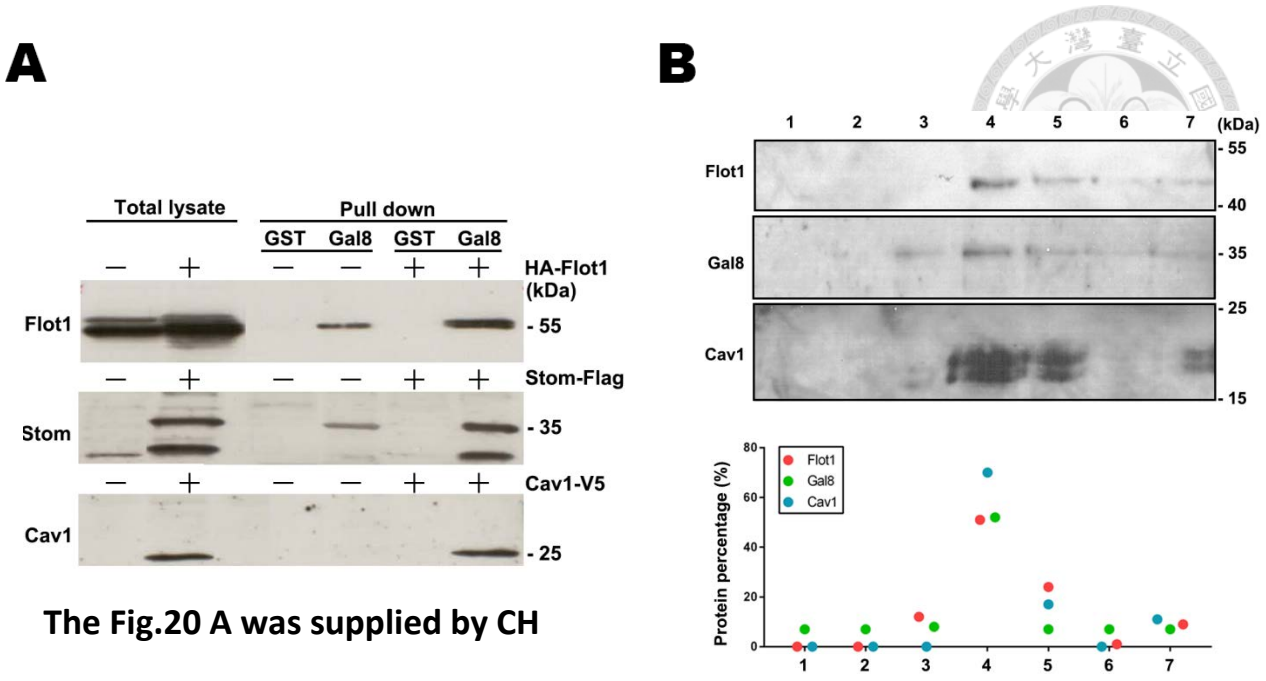

Fig. 20 Gal8 interacted and co-migrated with lipid raft scaffold proteins

(A) Cell lysates were collected from HEK293T cells over-expressing HA-tagged flotilin 1 (HA-Flot1), FLAG-tagged stomatin (Stom-FLAG) and V5-tagged caveolin 1 (Cav1-V5), respectively and mixed with GST or GST-Gal8 beads for pull down assay. (B) Polarized MDCK cells stably expressing FLAG-tagged galectin 8 were processed for lipid raft flotation assay. The distribution profile of the FLAG-Gal8 over the sucrose gradient was assessed by Western blotting using antibodies detecting FLAG-Gal8, Flot1, and Cav1.

doi:10.6342/NTU202302590

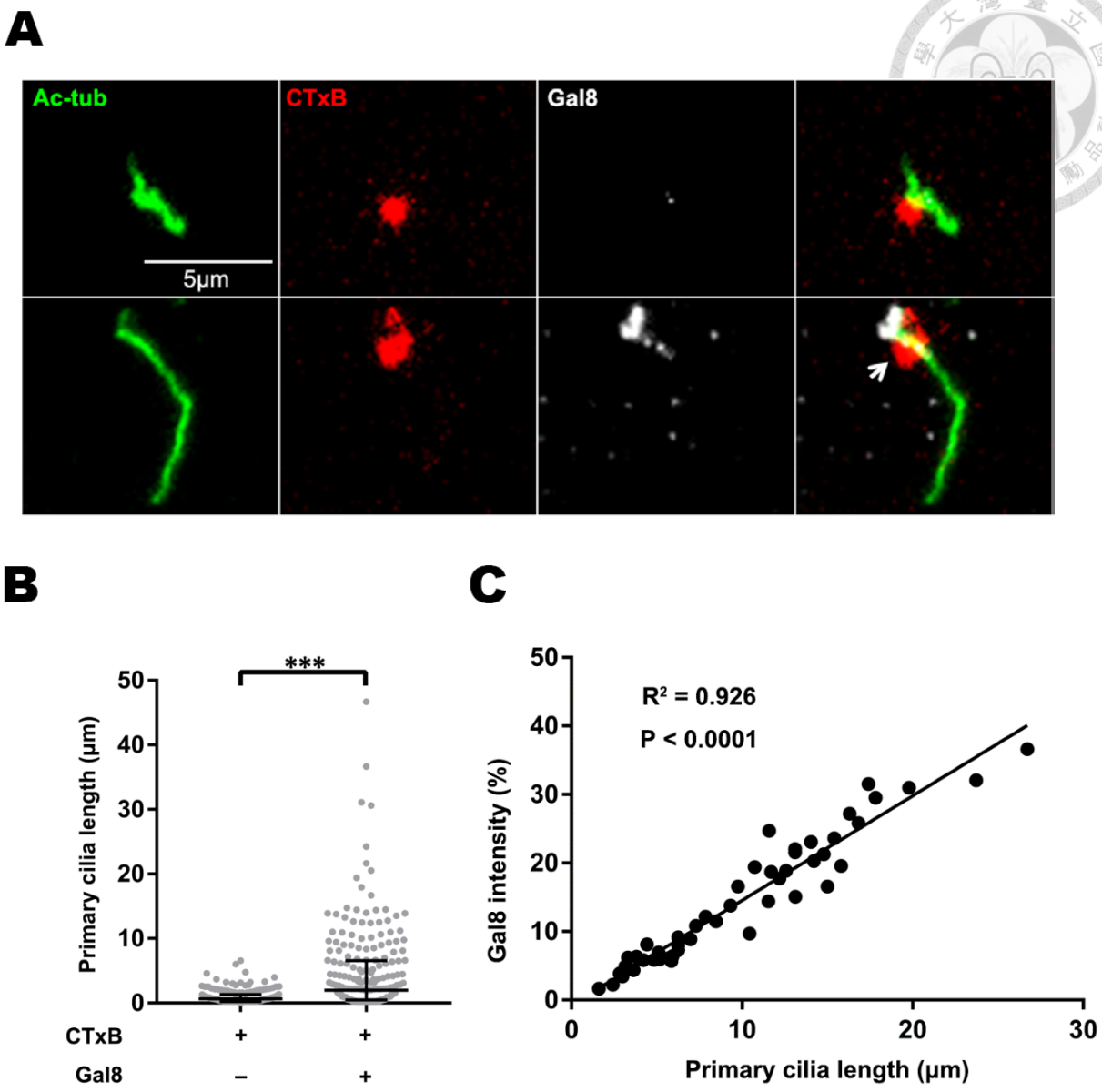

Fig. 21 Gal8 interacted with lipid raft on primary cilia.

(A,B) Polarized MDCK cells were treated with GST or GST-Gal8 (0.2 μg/μl), and processed for double immunofluorescence study with mouse anti-acetylated tubulin and rabbit anti-TMEM231 antibodies. (C) Correlation of the experimental results as described in panel A between the Gal8 fluorescent intensity colocalized with CTxB signal and the length of the respective cilium which was originated from the same region, n > 200.

doi:10.6342/NTU202302590

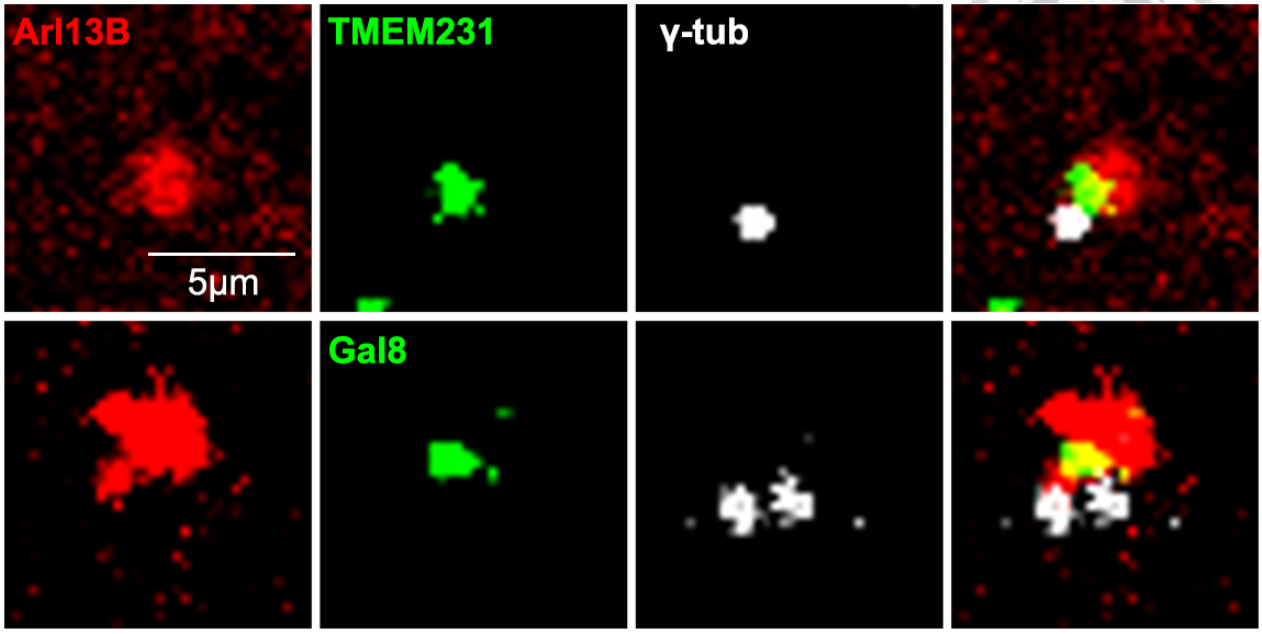

Fig. 22 Gal8 interacted with primary cilia at the transition zone.

Polarized MDCK cells were processed for apical labeling with Alexa-595 conjugated cholera toxin B subunit (CTxB) before double immunofluorescence study using rabbit anti-galectin 8 and mouse anti-acetylated tubulin antibodies.

doi:10.6342/NTU202302590

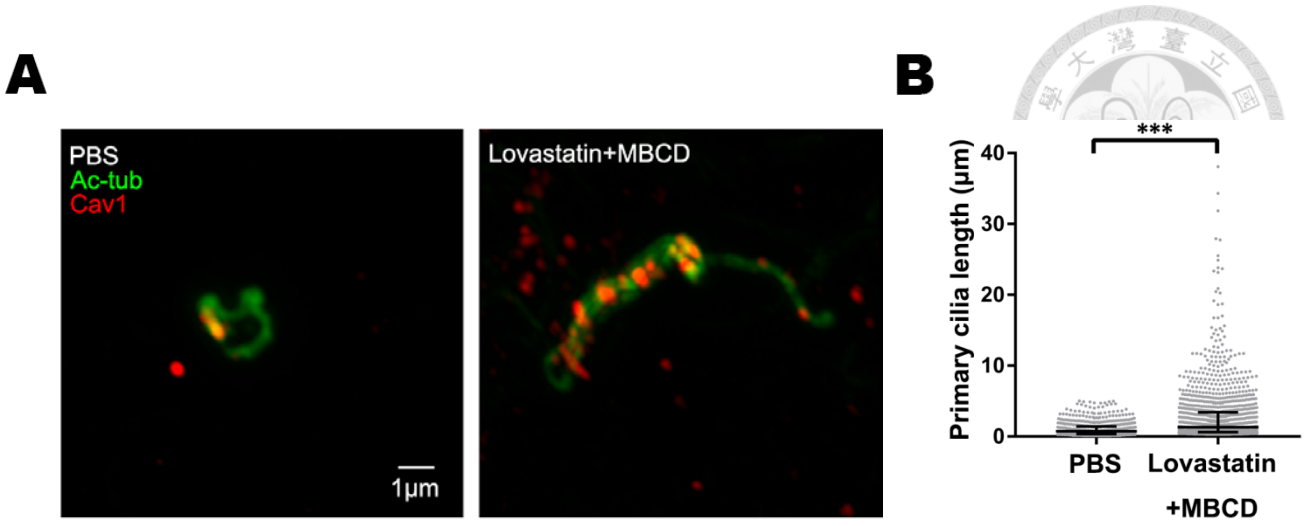

Fig. 23 Lipid raft disruption induced primary cilia elongation and caveolin 1 translocation. (A, B) Polarized MDCK cells were treated with lovastatin and methyl-beta-cyclodextrin (MBCD) before being processed for double immunofluorescence study using mouse anti-acetylated tubulin and rabbit anti-caveolin 1 (Cav1) antibodies to assess the expression pattern of Cav1 at primary cilia (A) and the length of primary cilia (B). The data were d quantified with nonparametric test, n > 200, ***P < 0.001.

doi:10.6342/NTU202302590

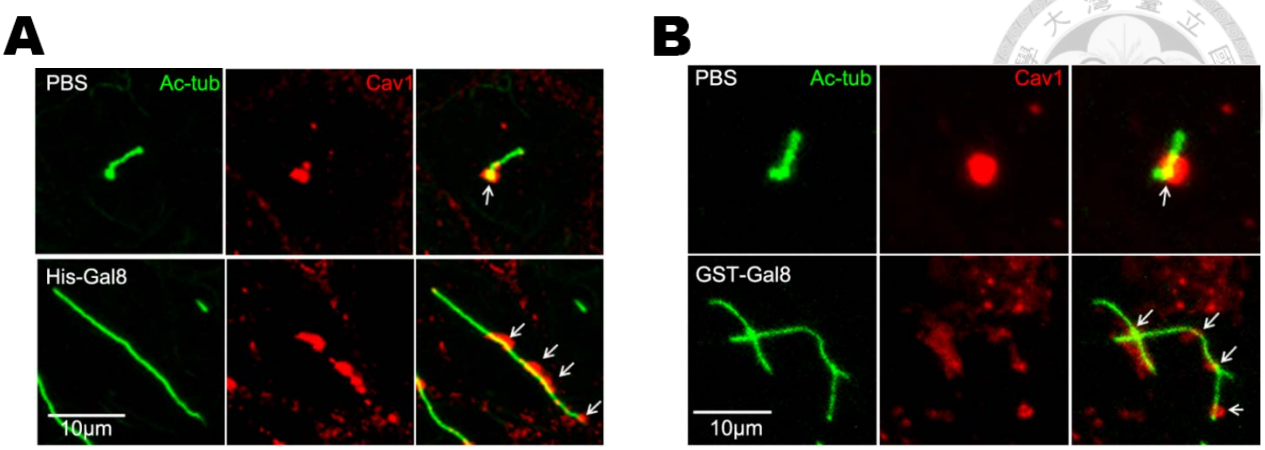

Fig. 24 Caveolin 1 is localized on primary cilia.

(A, B) Cav1 localization patterns at primary cilia in the control and 0.2 μg/μl recombinant His-Gal8 (A) or GST-Gal8 (B)-treated MDCK cells.

doi:10.6342/NTU202302590

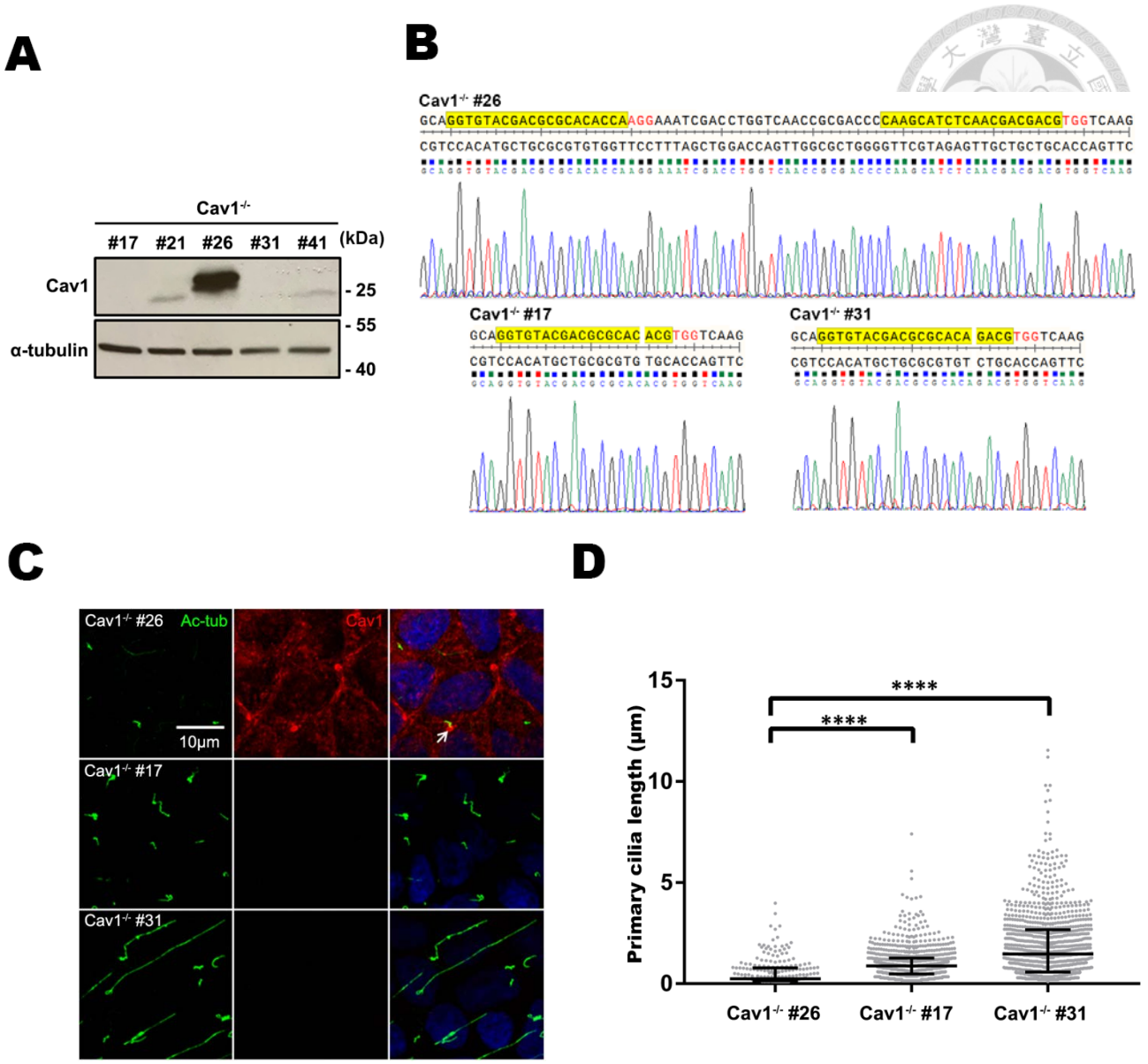

Fig. 25 Caveolin 1 depletion induced primary cilia elongation.

(A, B) CRISPR-Cas9 technique was used to generate caveolin 1 gene edited MDCK cells. Cav1 protein expression levels were analyzed in the indicated candidates by Western blotting analysis (A). Genome editing was confirmed by DNA sequencing across the single guided RNA targeted regions (highlighted in yellow) at the caveolin 1 genomic locus in selected clones (B). (C, D) Cav1 expression pattern (C) and the length of primary cilia (D) were shown in the indicated MDCK clones. The data were quantified with nonparametric test, n > 200, ****P < 0.0001 as compared to clone #26.

doi:10.6342/NTU202302590

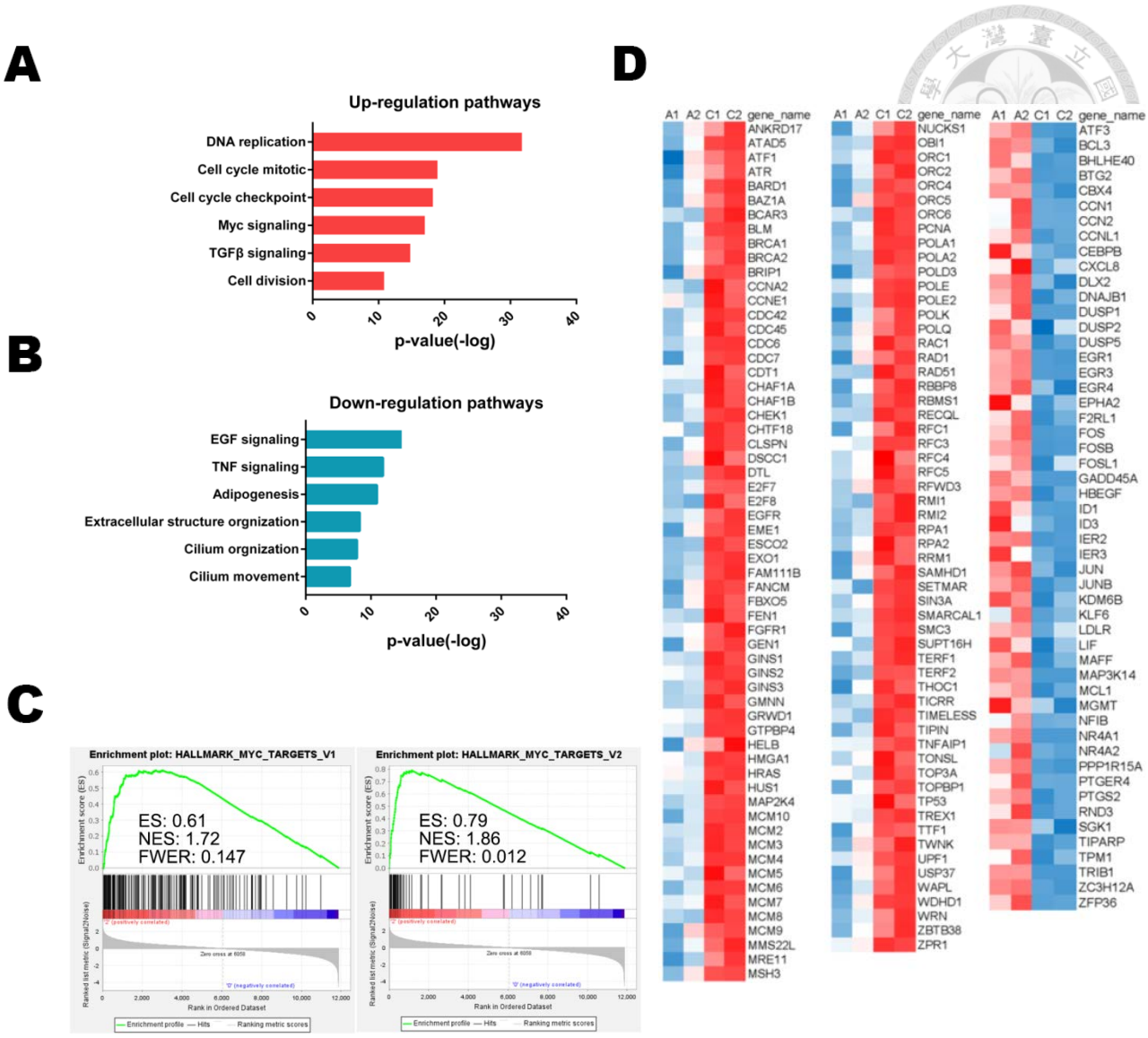

Fig. 26 Transcriptomic analysis of MDCK cells after Gal8 treatment.

After Gal8 treatment (0.2 μg/μl), several biological process were significantly (A) up-regulated and (B) down-regulated in curated gene-sets from online pathway databases were characterized by significance assessment by Fisher's exact test. (C) All transcriptomes were analyzed gene-level expression quantification using GSEA analysis with human MSigDB collections H (hallmark gene set) data base. (D) The heat map indicating the significantly quantitative alterations of representative genes was shown.

doi:10.6342/NTU202302590

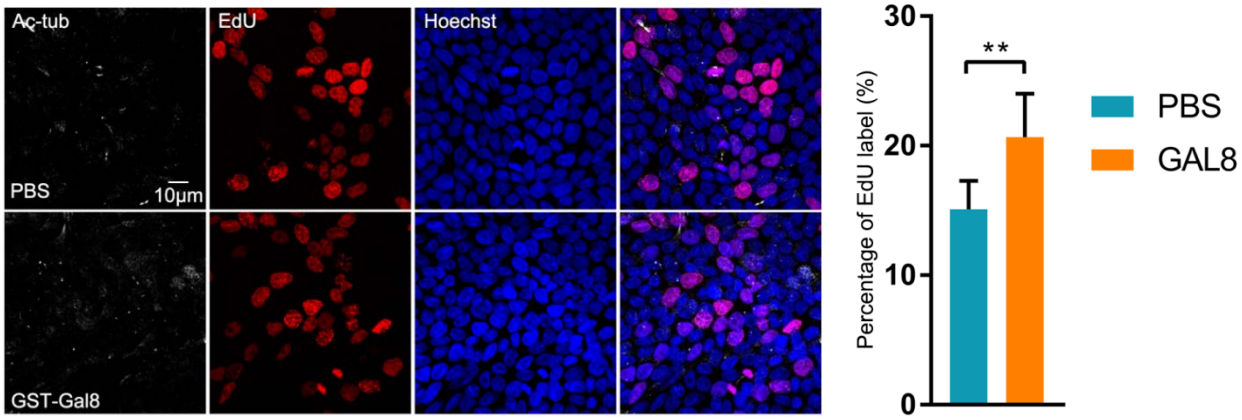

Fig. 27 Gal8 promote cell proliferation at early stage.

MDCK cells were treated with PBS or Gal8 (0.2 μg/μl) then EdU staining was used to label mitotic cells. The mitotic cells were quantified by Fiji image J particle analysis.

doi:10.6342/NTU202302590

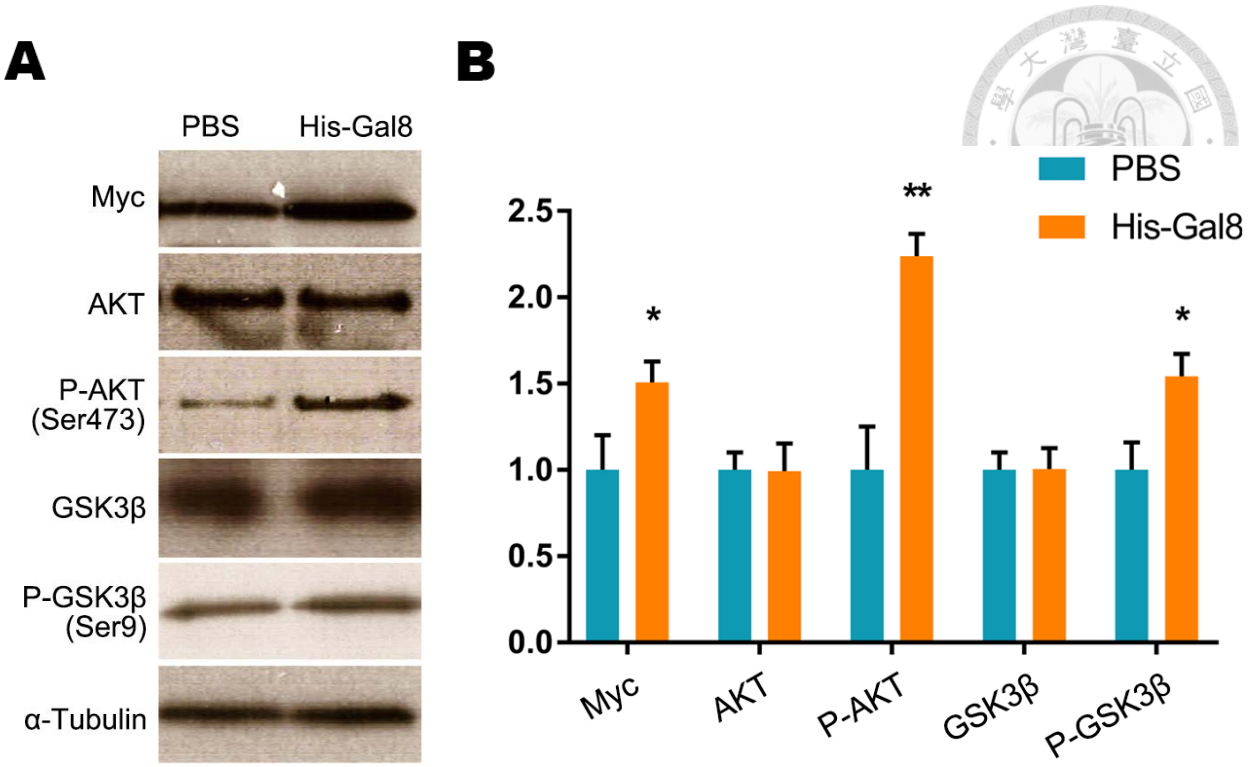

Fig. 28 Both of phosphorylated AKT and Myc protein levels were increased after Gal8 treatment.

(A) MDCK cells were treated with GST or GST-Gal8 (0.2 μg/μl)for 30 min on ice then recovery with fresh complete medium in 37°C for 5h. The cells were processed for Western blot analysis. (B) Quantification of the protein expressed level form (A).

doi:10.6342/NTU202302590

TABLES

Table 1. Candidate list for apical interacting partners of galectin 8

ID	Gene	Description	#Unique Peptides_Exp. 1	#Unique Peptides_Exp. 2	MW [kDa]
Q4PLA8	ABCB1	ATP binding cassette subfamily B member 1	14	44	141.6
F1PHV0	ABCC2	ATP binding cassette subfamily C member 2	7	12	173.8
F1PNA2	ABCC4	ATP binding cassette subfamily C member 4	12	27	149.5
F1PQ46	ANO6	anoctamin 6	2	5	100.6
F1P6B7	ANXA1	annexin A1	6	8	38.6
F1PBA1	ATP1A1	ATPase Na+/K+ transporting subunit alpha 1	17	38	112.6
J9P7J0	ATP1B1	ATPase Na+/K+ transporting subunit beta 1	2	3	28.8
E2QYG6	ATP6V1A	ATPase H+ transporting V1 subunit A	2	10	68.4
J9P3V6	BCAM	basal cell adhesion molecule (Lutheran blood group)	4	4	67.7
J9NVI2	BST2	bone marrow stromal cell antigen 2	3	3	20.6
J9P423	CD44	CD44 molecule (Indian blood group)	7	12	39.5
F1PGU2	CLCN6	chloride voltage-gated channel 6	2	9	97.2
J9NUV1	CLDN2	claudin 2	2	4	24.9
F1PHQ0	CLTC	clathrin heavy chain	4	34	191.5
E2R9S7	CTNNA1	catenin alpha 1	2	8	100.1
F1PW60	DSG1	desmoglein 1	9	10	113.8
E2RSI6	EZR	ezrin	5	11	69.4
F1PCK9	FAM234A	family with sequence similarity 234 member A	3	3	59.9
E2QSE3	FLOT1	flotillin 1	12	7	47.3

doi:10.6342/NTU202302590

ID	Gene	Description	#Unique Peptides_Exp. 1	#Unique Peptides_Exp. 2	MW [kDa]
F1PB95	ICAM1	intercellular adhesion molecule 1	2	4	58.1
F1PXU6	IGF1R	insulin like growth factor 1 receptor	21	16	154.8
E2REA9	ITGA2	integrin subunit alpha 2	8	9	129.6
F1Q439	ITGA3	integrin subunit alpha 3	6	3	116.7
F1P8Q0	ITGAV	integrin subunit alpha V	11	3	112.5
E2RT60	ITGB1	integrin subunit beta 1	6	8	88.1
A0A140T8E6	JUP	junction plakoglobin	20	26	81.7
F1Q260	LAMP1	lysosomal associated membrane protein 1	3	2	44.6
E2QWJ8	LAMTOR1	late endosomal/lysosomal adaptor, MAPK and MTOR activator 1	4	1	17.8
E2RQR4	LANCL1	LanC like 1	3	14	45.4
E2RKQ6	LGALS3BP	galectin 3 binding protein	3	7	62.2
E2R4Q1	LRP1	LDL receptor related protein 1	9	16	502.4
F1PAG7	LRPAP1	LDL receptor related protein associated protein 1	8	21	42.3
Z4YHE9	MET	MET proto-oncogene, receptor tyrosine kinase	5	2	151.1
E2RD92	MLEC	malectin	2	5	32.0
F1PZJ7	NIPSNAP2	nipsnap homolog 2	5	3	33.5
E2RJW8	PGRMC1	progesterone receptor membrane component 1	3	8	21.6
F1P9S5	PLXNB2	plexin B2	11	25	204.9
F1PR26	PTGFRN	prostaglandin F2 receptor inhibitor	17	6	97.1
E2R5J7	PTPRA	protein tyrosine phosphatase, receptor type A	3	12	89.6
F1PSB1	SEMA4D	semaphorin 4D	6	12	107.8
F1PY07	SIGIRR	single Ig and TIR domain containing	2	7	41.4

doi:10.6342/NTU202302590

ID	Gene	Description	#Unique Peptides_Exp. 1	#Unique Peptides_Exp. 2	MW [kDa]
F1P9W5	SLC12A2	solute carrier family 12 member 2	12	23	110.5
J9P6S2	SLC12A4	solute carrier family 12 member 4	4	9	119.7
F1Q2J3	SLC12A6	solute carrier family 12 member 6	6	13	127.7
F1PKH1	SLC12A7	solute carrier family 12 member 7	7	16	115.8
F1PCQ3	SLC16A1	solute carrier family 16 member 1	3	9	53.7
F1Q0H9	SLC1A4	solute carrier family 1 member 4	2	4	55.5
F1PPI5	SLC1A5	solute carrier family 1 member 5	4	8	57.5
F1PAM6	SLC27A4	solute carrier family 27 member 4	2	13	72.0
F1PWN2	SLC2A1	solute carrier family 2 member 1	2	3	54.1
F1PC23	SLC39A4	solute carrier family 39 member 4	4	7	62.7
F1P9U5	SLC44A4	solute carrier family 44 member 4	9	16	78.8
E2RCJ6	SLC4A2	solute carrier family 4 member 2	8	24	136.0
F1PTY0	SLC4A7	solute carrier family 4 member 7	3	12	138.0
E2R9T1	SLC5A6	solute carrier family 5 member 6	2	2	69.3
E2RGF3	SLC9A3R1	SLC9A3 regulator 1	3	11	39.6
F1PFS1	STOM	stomatin	9	9	25.6
A0A1W2NC67	STT3A	STT3 oligosaccharyltransferase complex catalytic subunit A	2	5	89.5
E2R4Q2	STX7	syntaxin 7	2	5	29.7

doi:10.6342/NTU202302590

ID	Gene	Description	#Unique Peptides_Exp. 1	#Unique Peptides_Exp. 2	MW [kDa]
F1PSP3	STX8	syntaxin 8	2	1	20.0
F1PZL2	TECR	trans-2,3-enoyl-CoA reductase	2	5	40.2
F1PIG4	TGM1	transglutaminase 1	7	7	90.6
E2RRB7	VAPB	VAMP associated protein B and C	2	4	27.1

doi:10.6342/NTU202302590

Table 2. Candidate list for gene expression induced by galectin 8

Please check this link: https://140.112.133.21:7733/sharing/ifibwDPSS

doi:10.6342/NTU202302590

RFERENCES

1. Satir P and Christensen ST (2007) Overview of structure and function of mammalian cilia. Annu Rev Physiol 69:377-400. https://doi.org/10.1146/annurev.physiol.69.040705.141236
2. Besschetnova TY, Kolpakova-Hart E, Guan Y et al. (2010) Identification of signaling pathways regulating primary cilium length and flow-mediated adaptation. Curr Biol 20:182-7. https://doi.org/10.1016/j.cub.2009.11.072
3. Sorokin S (1962) Centrioles and the formation of rudimentary cilia by fibroblasts and smooth muscle cells. J Cell Biol 15:363-77. https://doi.org/10.1083/jcb.15.2.363
4. Sorokin SP (1968) Reconstructions of centriole formation and ciliogenesis in mammalian lungs. J Cell Sci 3:207-30. https://doi.org/10.1242/jcs.3.2.207
5. Dawe HR, Smith UM, Cullinane AR et al. (2007) The Meckel-Gruber Syndrome proteins MKS1 and meckelin interact and are required for primary cilium formation. Hum Mol Genet 16:173-86. https://doi.org/10.1093/hmg/ddl459
6. Dawe HR, Adams M, Wheway G et al. (2009) Nesprin-2 interacts with meckelin and mediates ciliogenesis via remodelling of the actin cytoskeleton. J Cell Sci 122:2716-26. https://doi.org/10.1242/jcs.043794
7. Lemullois M, Boisvieux-Ulrich E, Laine MC et al. (1988) Development and functions of the cytoskeleton during ciliogenesis in metazoa. Biol Cell 63:195-208. https://doi.org/10.1016/0248-4900(88)90058-5
8. Follit JA, Tuft RA, Fogarty KE et al. (2006) The intraflagellar transport protein IFT20 is associated with the Golgi complex and is required for cilia assembly. Mol Biol Cell 17:3781-92. https://doi.org/10.1091/mbc.e06-02-0133
9. Nachury MV, Loktev AV, Zhang Q et al. (2007) A core complex of BBS proteins cooperates with the GTPase Rab8 to promote ciliary membrane biogenesis. Cell 129:1201-13. https://doi.org/10.1016/j.cell.2007.03.053
10. Westlake CJ, Baye LM, Nachury MV et al. (2011) Primary cilia membrane assembly is initiated by Rab11 and transport protein particle II (TRAPPII) complex-dependent trafficking of Rabin8 to the centrosome. Proc Natl Acad Sci U S A 108:2759-64. https://doi.org/10.1073/pnas.1018823108
11. Rosenbaum JL and Witman GB (2002) Intraflagellar transport. Nat Rev Mol Cell Biol 3:813-25. https://doi.org/10.1038/nrm952
12. Taschner M and Lorentzen E (2016) The Intraflagellar Transport Machinery. Cold Spring Harb Perspect Biol 8:a028092. https://doi.org/10.1101/cshperspect.a028092
13. Marshall WF and Rosenbaum JL (2001) Intraflagellar transport balances continuous turnover of outer doublet microtubules: implications for flagellar length control. J Cell Biol 155:405-14. https://doi.org/10.1083/jcb.200106141
14. Engel BD, Ludington WB and Marshall WF (2009) Intraflagellar transport particle size scales

doi:10.6342/NTU202302590

inversely with flagellar length: revisiting the balance-point length control model. J Cell Biol 187:81-9. https://doi.org/10.1083/jcb.200812084
15. Ludington WB, Wemmer KA, Lechtreck KF et al. (2013) Avalanche-like behavior in ciliary import. PNAS 110:3925-30. https://doi.org/10.1073/pnas.1217354110
16. Wren KN, Craft JM, Tritschler D et al. (2013) A differential cargo-loading model of ciliary length regulation by IFT. Curr Biol 23:2463-71. https://doi.org/10.1016/j.cub.2013.10.044
17. Craft JM, Harris JA, Hyman S et al. (2015) Tubulin transport by IFT is upregulated during ciliary growth by a cilium-autonomous mechanism. J Cell Biol 208:223-37. https://doi.org/10.1083/jcb.201409036
18. Reiter JF, Blacque OE and Leroux MR (2012) The base of the cilium: roles for transition fibres and the transition zone in ciliary formation, maintenance and compartmentalization. EMBO Rep 13:608-18. https://doi.org/10.1038/embor.2012.73
19. Garcia-Gonzalo FR and Reiter JF (2012) Scoring a backstage pass: mechanisms of ciliogenesis and ciliary access. J Cell Biol 197:697-709. https://doi.org/10.1083/jcb.201111146
20. Goncalves J and Pelletier L (2017) The Ciliary Transition Zone: Finding the Pieces and Assembling the Gate. Mol Cells 40:243-53. https://doi.org/10.14348/molcells.2017.0054
21. O'Toole ET, Giddings TH, Jr. and Dutcher SK (2007) Understanding microtubule organizing centers by comparing mutant and wild-type structures with electron tomography. Methods Cell Biol 79:125-43. https://doi.org/10.1016/S0091-679X(06)79005-7
22. Quinlan RJ, Tobin JL and Beales PL (2008) Modeling ciliopathies: Primary cilia in development and disease. Curr Top Dev Biol 84:249-310. https://doi.org/10.1016/S0070-2153(08)00605-4
23. Liu Q, Tan G, Levenkova N et al. (2007) The proteome of the mouse photoreceptor sensory cilium complex. Mol Cell Proteomics 6:1299-317. https://doi.org/10.1074/mcp.M700054-MCP200
24. Garcia-Gonzalo FR, Corbit KC, Sirerol-Piquer MS et al. (2011) A transition zone complex regulates mammalian ciliogenesis and ciliary membrane composition. Nat Genet 43:776-84. https://doi.org/10.1038/ng.891
25. Schou KB, Mogensen JB, Morthorst SK et al. (2017) KIF13B establishes a CAV1-enriched microdomain at the ciliary transition zone to promote Sonic hedgehog signalling. Nat Commun 8:14177. https://doi.org/10.1038/ncomms14177
26. Ringo DL (1967) Flagellar motion and fine structure of the flagellar apparatus in Chlamydomonas. J Cell Biol 33:543-71. https://doi.org/10.1083/jcb.33.3.543
27. Janich P and Corbeil D (2007) GM1 and GM3 gangliosides highlight distinct lipid microdomains within the apical domain of epithelial cells. FEBS Lett 581:1783-7. https://doi.org/10.1016/j.febslet.2007.03.065
28. Yamakawa D, Katoh D, Kasahara K et al. (2021) Primary cilia-dependent lipid raft/caveolin dynamics regulate adipogenesis. Cell Rep 34:108817. https://doi.org/10.1016/j.celrep.2021.108817
29. Carlsson S, Oberg CT, Carlsson MC et al. (2007) Affinity of galectin-8 and its carbohydrate

doi:10.6342/NTU202302590

recognition domains for ligands in solution and at the cell surface. Glycobiology 17:663-76. https://doi.org/10.1093/glycob/cwm026
30. Elola MT, Ferragut F, Cardenas Delgado VM et al. (2014) Expression, localization and function of galectin-8, a tandem-repeat lectin, in human tumors. Histol Histopathol 29:1093-105. https://doi.org/10.14670/HH-29.1093
31. Poland PA, Rondanino C, Kinlough CL et al. (2011) Identification and characterization of endogenous galectins expressed in Madin Darby canine kidney cells. J Biol Chem 286:6780-90. https://doi.org/10.1074/jbc.M110.179002
32. Kasai K, Oda Y, Nishikata M et al. (1986) Frontal affinity chromatography: theory for its application to studies on specific interactions of biomolecules. J Chromatogr 376:33-47. https://doi.org/10.1016/s0378-4347(00)80822-1
33. Hirabayashi J, Hashidate T, Arata Y et al. (2002) Oligosaccharide specificity of galectins: a search by frontal affinity chromatography. Biochim Biophys Acta 1572:232-54. https://doi.org/10.1016/s0304-4165(02)00311-2
34. Ideo H, Matsuzaka T, Nonaka T et al. (2011) Galectin-8-N-domain recognition mechanism for sialylated and sulfated glycans. J Biol Chem 286:11346-55. https://doi.org/10.1074/jbc.M110.195925
35. Lim H, Yu CY and Jou TS (2017) Galectin-8 regulates targeting of Gp135/podocalyxin and lumen formation at the apical surface of renal epithelial cells. FASEB J 31:4917-27. https://doi.org/10.1096/fj.201601386R
36. Li FY, Weng IC, Lin CH et al. (2019) Helicobacter pylori induces intracellular galectin-8 aggregation around damaged lysosomes within gastric epithelial cells in a host O-glycan-dependent manner. Glycobiology 29:151-62. https://doi.org/10.1093/glycob/cwy095
37. Obino D, Fetler L, Soza A et al. (2018) Galectin-8 Favors the Presentation of Surface-Tethered Antigens by Stabilizing the B Cell Immune Synapse. Cell Rep 25:3110-22 e6. https://doi.org/10.1016/j.celrep.2018.11.052
38. Porebska N, Pozniak M, Matynia A et al. (2021) Galectins as modulators of receptor tyrosine kinases signaling in health and disease. Cytokine Growth Factor Rev 60:89-106. https://doi.org/10.1016/j.cytogfr.2021.03.004
39. Meinohl C, Barnard SJ, Fritz-Wolf K et al. (2019) Galectin-8 binds to the Farnesylated C-terminus of K-Ras4B and Modifies Ras/ERK Signaling and Migration in Pancreatic and Lung Carcinoma Cells. Cancers (Basel) 12. https://doi.org/10.3390/cancers12010030
40. Anvarian Z, Mykytyn K, Mukhopadhyay S et al. (2019) Cellular signalling by primary cilia in development, organ function and disease. Nat Rev Nephrol 15:199-219. https://doi.org/10.1038/s41581-019-0116-9
41. Corbit KC, Aanstad P, Singla V et al. (2005) Vertebrate Smoothened functions at the primary cilium. Nature 437:1018-21. https://doi.org/10.1038/nature04117
42. Haycraft CJ, Banizs B, Aydin-Son Y et al. (2005) Gli2 and Gli3 localize to cilia and require the

doi:10.6342/NTU202302590

intraflagellar transport protein polaris for processing and function. PLoS Genet 1:e53. https://doi.org/10.1371/journal.pgen.0010053

43. Bergmann C, Fliegauf M, Bruchle NO et al. (2008) Loss of nephrocystin-3 function can cause embryonic lethality, Meckel-Gruber-like syndrome, situs inversus, and renal-hepatic-pancreatic dysplasia. Am J Hum Genet 82:959-70. https://doi.org/10.1016/j.ajhg.2008.02.017
44. Lancaster MA, Schroth J and Gleeson JG (2011) Subcellular spatial regulation of canonical Wnt signalling at the primary cilium. Nat Cell Biol 13:700-7. https://doi.org/10.1038/ncb2259
45. Dalbay MT, Thorpe SD, Connelly JT et al. (2015) Adipogenic Differentiation of hMSCs is Mediated by Recruitment of IGF-1r Onto the Primary Cilium Associated With Cilia Elongation. Stem Cells 33:1952-61. https://doi.org/10.1002/stem.1975
46. Zhu D, Shi S, Wang H et al. (2009) Growth arrest induces primary-cilium formation and sensitizes IGF-1-receptor signaling during differentiation induction of 3T3-L1 preadipocytes. J Cell Sci 122:2760-8. https://doi.org/10.1242/jcs.046276
47. Heydeck W, Fievet L, Davis EE et al. (2018) The complexity of the cilium: spatiotemporal diversity of an ancient organelle. Curr Opin Cell Biol 55:139-49. https://doi.org/10.1016/j.ceb.2018.08.001
48. Liu CH, Huang ZH, Huang SC et al. (2021) Endocytosis of peroxiredoxin 1 links sterile inflammation to immunoparalysis in pediatric patients following cardiopulmonary bypass. Redox Biol 46:102086. https://doi.org/10.1016/j.redox.2021.102086
49. Liu PJ, Chen CD, Wang CL et al. (2015) In-depth proteomic analysis of six types of exudative pleural effusions for nonsmall cell lung cancer biomarker discovery. Mol Cell Proteomics 14:917-32. https://doi.org/10.1074/mcp.M114.045914
50. Wang YH, Chiu WY, Chen YT et al. (2022) Golgin Imh1 and GARP complex cooperate to restore the impaired SNARE recycling transport induced by ER stress. Cell Rep 38:110488. https://doi.org/10.1016/j.celrep.2022.110488
51. Perez-Riverol Y, Bai J, Bandla C et al. (2022) The PRIDE database resources in 2022: a hub for mass spectrometry-based proteomics evidences. Nucleic Acids Res 50:D543-D52. https://doi.org/10.1093/nar/gkab1038
52. Popa SJ, Stewart SE and Moreau K (2018) Unconventional secretion of annexins and galectins. Semin Cell Dev Biol 83:42-50. https://doi.org/10.1016/j.semcdb.2018.02.022
53. Han SJ, Jang HS, Kim JI et al. (2016) Unilateral nephrectomy elongates primary cilia in the remaining kidney via reactive oxygen species. Sci Rep 6:22281. https://doi.org/10.1038/srep22281
54. Chen JY, Lin YY and Jou TS (2012) Phosphorylation of EBP50 negatively regulates beta-PIX-dependent Rac1 activity in anoikis. Cell Death Differ 19:1027-37. https://doi.org/10.1038/cdd.2012.4
55. Kolter T (2012) Ganglioside biochemistry. ISRN Biochem 2012:506160. https://doi.org/10.5402/2012/506160
56. Schnaar RL, Gerardy-Schahn R and Hildebrandt H (2014) Sialic acids in the brain: gangliosides

doi:10.6342/NTU202302590

and polysialic acid in nervous system development, stability, disease, and regeneration. Physiol Rev 94:461-518. https://doi.org/10.1152/physrev.00033.2013

57. Prinetti A, Chigorno V, Tettamanti G et al. (2000) Sphingolipid-enriched membrane domains from rat cerebellar granule cells differentiated in culture. A compositional study. J Biol Chem 275:11658-65. https://doi.org/10.1074/jbc.275.16.11658
58. Dutta P and Ray K (2022) Ciliary membrane, localised lipid modification and cilia function. J Cell Physiol 237:2613-31. https://doi.org/10.1002/jcp.30787
59. Roberson EC, Dowdle WE, Ozanturk A et al. (2015) TMEM231, mutated in orofaciodigital and Meckel syndromes, organizes the ciliary transition zone. J Cell Biol 209:129-42. https://doi.org/10.1083/jcb.201411087
60. Lambacher NJ, Bruel AL, van Dam TJ et al. (2016) TMEM107 recruits ciliopathy proteins to subdomains of the ciliary transition zone and causes Joubert syndrome. Nat Cell Biol 18:122-31. https://doi.org/10.1038/ncb3273
61. Jauregui AR, Nguyen KC, Hall DH et al. (2008) The Caenorhabditis elegans nephrocystins act as global modifiers of cilium structure. J Cell Biol 180:973-88. https://doi.org/10.1083/jcb.200707090
62. Li C, Jensen VL, Park K et al. (2016) MKS5 and CEP290 Dependent Assembly Pathway of the Ciliary Transition Zone. PLoS Biol 14:e1002416. https://doi.org/10.1371/journal.pbio.1002416
63. Huang L, Szymanska K, Jensen VL et al. (2011) TMEM237 is mutated in individuals with a Joubert syndrome related disorder and expands the role of the TMEM family at the ciliary transition zone. Am J Hum Genet 89:713-30. https://doi.org/10.1016/j.ajhg.2011.11.005
64. Jensen VL, Li C, Bowie RV et al. (2015) Formation of the transition zone by Mks5/Rpgrip1L establishes a ciliary zone of exclusion (CIZE) that compartmentalises ciliary signalling proteins and controls PIP2 ciliary abundance. EMBO J 34:2537-56. https://doi.org/10.15252/embj.201488044
65. Williams CL, Li C, Kida K et al. (2011) MKS and NPHP modules cooperate to establish basal body/transition zone membrane associations and ciliary gate function during ciliogenesis. J Cell Biol 192:1023-41. https://doi.org/10.1083/jcb.201012116
66. Rangel L, Bernabe-Rubio M, Fernandez-Barrera J et al. (2019) Caveolin-1alpha regulates primary cilium length by controlling RhoA GTPase activity. Sci Rep 9:1116. https://doi.org/10.1038/s41598-018-38020-5
67. Scheidel N, Kennedy J and Blacque OE (2018) Endosome maturation factors Rabenosyn-5/VPS45 and caveolin-1 regulate ciliary membrane and polycystin-2 homeostasis. EMBO J 37:e98248. https://doi.org/10.15252/embj.201798248
68. Ferragut F, Cagnoni AJ, Colombo LL et al. (2019) Dual knockdown of Galectin-8 and its glycosylated ligand, the activated leukocyte cell adhesion molecule (ALCAM/CD166), synergistically delays in vivo breast cancer growth. Biochim Biophys Acta Mol Cell Res 1866:1338-52. https://doi.org/10.1016/j.bbamcr.2019.03.010

doi:10.6342/NTU202302590

69. Cocucci E and Meldolesi J (2015) Ectosomes and exosomes: shedding the confusion between extracellular vesicles. Trends Cell Biol 25:364-72. https://doi.org/10.1016/j.tcb.2015.01.004
70. Dolo V, Ginestra A, Cassara D et al. (1998) Selective localization of matrix metalloproteinase 9, beta1 integrins, and human lymphocyte antigen class I molecules on membrane vesicles shed by 8701-BC breast carcinoma cells. Cancer Res 58:4468-74.
71. Stec M, Baj-Krzyworzeka M, Baran J et al. (2015) Isolation and characterization of circulating micro(nano)vesicles in the plasma of colorectal cancer patients and their interactions with tumor cells. Oncol Rep 34:2768-75. https://doi.org/10.3892/or.2015.4228
72. Berchem G, Noman MZ, Bosseler M et al. (2016) Hypoxic tumor-derived microvesicles negatively regulate NK cell function by a mechanism involving TGF-beta and miR23a transfer. Oncoimmunology 5:e1062968. https://doi.org/10.1080/2162402X.2015.1062968
73. Del Conde I, Shrimpton CN, Thiagarajan P et al. (2005) Tissue-factor-bearing microvesicles arise from lipid rafts and fuse with activated platelets to initiate coagulation. Blood 106:1604-11. https://doi.org/10.1182/blood-2004-03-1095
74. Jaiswal R, Luk F, Dalla PV et al. (2013) Breast cancer-derived microparticles display tissue selectivity in the transfer of resistance proteins to cells. PLoS One 8:e61515. https://doi.org/10.1371/journal.pone.0061515
75. Pokharel D, Padula MP, Lu JF et al. (2014) Proteome analysis of multidrug-resistant, breast cancer-derived microparticles. J Extracell Vesicles 3. https://doi.org/10.3402/jev.v3.24384
76. Stewart SE, Ashkenazi A, Williamson A et al. (2018) Transbilayer phospholipid movement facilitates the translocation of annexin across membranes. J Cell Sci 131:jcs217034. https://doi.org/10.1242/jcs.217034
77. Forschbach V, Goppelt-Struebe M, Kunzelmann K et al. (2015) Anoctamin 6 is localized in the primary cilium of renal tubular cells and is involved in apoptosis-dependent cyst lumen formation. Cell Death Dis 6:e1899. https://doi.org/10.1038/cddis.2015.273
78. Wein S, Fauroux M, Laffitte J et al. (2004) Mediation of annexin 1 secretion by a probenecid-sensitive ABC-transporter in rat inflamed mucosa. Biochem Pharmacol 67:1195-202. https://doi.org/10.1016/j.bcp.2003.11.015
79. Chapman LP, Epton MJ, Buckingham JC et al. (2003) Evidence for a role of the adenosine 5'-triphosphate-binding cassette transporter A1 in the externalization of annexin I from pituitary folliculo-stellate cells. Endocrinology 144:1062-73. https://doi.org/10.1210/en.2002-220650
80. Yabas M, Jing W, Shafik S et al. (2016) ATP11C Facilitates Phospholipid Translocation across the Plasma Membrane of All Leukocytes. PLoS One 11:e0146774. https://doi.org/10.1371/journal.pone.0146774
81. Nitulescu GM, Van De Venter M, Nitulescu G et al. (2018) The Akt pathway in oncology therapy and beyond (Review). Int J Oncol 53:2319-31. https://doi.org/10.3892/ijo.2018.4597
82. Christensen ST, Clement CA, Satir P et al. (2012) Primary cilia and coordination of receptor tyrosine kinase (RTK) signalling. J Pathol 226:172-84. https://doi.org/10.1002/path.3004

doi:10.6342/NTU202302590

83. Wang H, Zou X, Wei Z et al. (2015) Hsp90alpha forms a stable complex at the cilium neck for the interaction of signalling molecules in IGF-1 receptor signalling. J Cell Sci 128:100-8. https://doi.org/10.1242/jcs.155101
84. Stilling S, Kalliakoudas T, Benninghoven-Frey H et al. (2022) PIP(2) determines length and stability of primary cilia by balancing membrane turnovers. Commun Biol 5:93. https://doi.org/10.1038/s42003-022-03028-1
85. Czech MP (2000) PIP2 and PIP3: complex roles at the cell surface. Cell 100:603-6. https://doi.org/10.1016/s0092-8674(00)80696-0

doi:10.6342/NTU202302590